Garnet Granulite Xenoliths from the Northern Baltic Shield--the Underplated Lower Crust of a Palaeoproterozoic Large Igneous Province?

Article *in* Journal of Petrology · January 2001

DOI: 10.1093/petrology/42.4.731 · Source: OAI

CITATIONS
78

READS
195

6 authors, including:

Pamela Kempton
Kansas State University
180 PUBLICATIONS **7,756** CITATIONS
SEE PROFILE

Hilary Downes
Birkbeck, University of London
266 PUBLICATIONS **9,106** CITATIONS
SEE PROFILE

Leonid A. Neymark
United States Geological Survey Denver CO
156 PUBLICATIONS **1,760** CITATIONS
SEE PROFILE

Jo-Anne Wartho
GEOMAR Helmholtz Centre for Ocean Research Kiel
118 PUBLICATIONS **2,392** CITATIONS
SEE PROFILE

JOURNAL OF PETROLOGY | VOLUME 42 | NUMBER 4 | PAGES 731–763 | 2001

Garnet Granulite Xenoliths from the Northern Baltic Shield—the Underplated Lower Crust of a Palaeoproterozoic Large Igneous Province?

P. D. KEMPTON[1]*, H. DOWNES[2], L. A. NEYMARK[3], J. A. WARTHO[4], R. E. ZARTMAN[5]† AND E. V. SHARKOV[6]

[1]NERC ISOTOPE GEOSCIENCES LABORATORY, KINGSLEY DUNHAM CENTRE, KEYWORTH NG12 5GG, UK

[2]BIRKBECK/UCL RESEARCH SCHOOL OF GEOLOGICAL AND GEOPHYSICAL SCIENCES, BIRKBECK COLLEGE, MALET STREET, LONDON WC1E 7HX, UK

[3]US GEOLOGICAL SURVEY, DFC, BOX 25046, MS 963, DENVER, CO, USA

[4]DEPARTMENT OF EARTH SCIENCES, OPEN UNIVERSITY, WALTON HALL, MILTON KEYNES MK7 6AA, UK

[5]DEPARTMENT OF GEOLOGICAL SCIENCES, UNIVERSITY OF CAPE TOWN, RONDEBOSCH 7700, SOUTH AFRICA

[6]IGEM, STAROMONETNY PER 35, MOSCOW, 109017, RUSSIA

RECEIVED JULY 14, 1999; REVISED TYPESCRIPT ACCEPTED JULY 12, 2000

Garnet granulite facies xenoliths hosted in Devonian lamprophyres from the Kola Peninsula are interpreted to represent the high-grade metamorphic equivalents of continental flood tholeiites, emplaced into the Baltic Shield Archaean lower crust in early Proterozoic time. Geochronological data and similarities in major and trace element geochemistry suggest that the xenoliths formed during the same plume-related magmatic event that created a widespread Palaeoproterozoic large igneous province (LIP) at 2·4–2·5 Ga. They are, thus, the first samples of the lower crust of a Palaeoproterozoic LIP to be studied in petrological detail. The suite includes mafic granulites (gar + cpx + rutile ± plag ± opx ± phlog ± amph), felsic granulites (plag + gar + cpx + rutile ± qtz ± Kspar ± phlog ± amph) and pyroxenites (± phlog ± amph), but mafic garnet granulites predominate. Although some samples are restites, there is no evidence for a predominance of magmatic cumulates, as is common for Phanerozoic lower-crustal xenolith suites. Metasediments are also absent. Phlogopite and/or amphibole occur in xenoliths of all types and are interpreted to be metasomatic in origin. The K-rich metasomatic event occurred at ~2·0 Ga, and led to substantial enrichment in Rb, K, LREE/HREE, Th/U, Th/Pb and, to a lesser extent, Nb and Ti. The fluids responsible for this metasomatism were probably derived from a second plume that arrived beneath the region at this time. Evidence for partial melting of mafic crust exists in the presence of migmatitic granulites. The timing of migmatization overlaps that of metasomatism, and it is suggested that migmatization was facilitated by the metasomatism. The metamorphism, metasomatism and migmatization recorded in the Kola granulite xenoliths may be representative of the processes responsible for converting Archaean LIP-generated proto-continents into continental crust.

KEY WORDS: *granulite xenoliths; metasomatism; migmatization; Sr–Nd–Pb isotopes; geochronology*

INTRODUCTION

A crucial unresolved question of crustal evolution is whether the processes that formed the lower continental crust in Archaean–Proterozoic times were similar to those that have operated during the Phanerozoic. It is generally believed that growth of continental crust has occurred

Extended dataset can be found at:
http://www.petrology.oupjournals.org

*Corresponding author. E-mail: p.kempton@nigl.nerc.ac.uk
†Present address: Department of Cosmochemistry, Max-Planck-Institute for Chemistry, PO Box 3060, D-55020 Mainz, Germany.

through either or both of two mechanisms: volcanic arc accretion (Taylor, 1967, 1977) or magmatism associated with large igneous provinces (LIP), such as oceanic plateaux (Stein & Hofmann, 1994; Abbott & Mooney, 1995; Stein & Goldstein, 1996). The arc accretion model is of long standing and requires no further explanation here. The more recent LIP model suggests that growth of the continental crust may be connected to the presence of mantle plumes, particularly if accompanied by rifting (e.g. White *et al.*, 1987). The plume model may therefore be able to explain periods of rapid continental growth better than the volcanic arc accretion model. Regardless of which mechanism predominates, differentiation and modification of juvenile crust must be an important process in creating the enrichment of silica and various incompatible trace elements observed in the continental crust, because the magmatic input for both primitive mantle-derived arcs and oceanic plateaux is largely mafic (White *et al.*, 1999).

Information about the lower crust is essential if we are to fully understand the processes of continental growth and evolution. Only direct samples of the lower crust, in the form of xenoliths entrained in mafic alkaline magmas, can yield unambiguous information about its mineralogy and chemical composition—and ultimately answer questions concerning its age, origin and evolution. However, although lower-crustal xenoliths are abundant from crust that was consolidated in Phanerozoic times (Rudnick, 1992; Downes, 1993), xenoliths from the lower crust beneath Archaean–Proterozoic cratonic regions are much less common. We present here a study of a Proterozoic xenolith suite from the northern Baltic Shield, brought to the surface by a Devonian ultramafic lamprophyre diatreme. The Archaean–Proterozoic craton of the northern Baltic Shield has remained unaffected by major orogenic events since mid-Proterozoic times, as demonstrated by the existence of flat-lying sediments of Riphean (0·9–1·4 Ga) age (Mitrofanov, 1995). The crust has also remained relatively thick, reaching 42–46 km in the region of the Gulf of Kandalaksha (Azbel *et al.*, 1989). Thus, the area represents an excellent locality for the study of the processes involved in the formation and evolution of old cratonic lower crust.

GEOLOGICAL BACKGROUND

The ultramafic lamprophyre diatreme from which the majority of the xenoliths were collected is situated on Elovy island, located in the Kandalaksha Gulf at the western end of the White Sea, Kola Peninsula (Fig. 1a). An additional xenolith, Sample 67-12, comes from a dyke on the nearby Middle Salni Island.

The Kola Peninsula is dominated by Archaean and Proterozoic rocks ranging in age from 2·9 to 1·7 Ga. The diatremes in which the xenoliths are found erupted through the Belomorian Mobile Belt—a transition (or suture) zone between the 3·2–2·8 Ga Karelian granite–greenstone terrane in the southwest and the 3·0–2·7 Ga Kola granulite gneiss province in the northeast (Fig. 1b). The Belomorian Mobile Belt is composed predominantly of 2·9–2·4 Ga tonalite–trondhjemite gneisses, metasediments, amphibolites and migmatites reworked from the granite–greenstone lithologies of the adjacent Karelian block.

The region was once part of a much larger continental mass that existed between 2·7 and 2·5 Ga, and consisted of the present-day Canadian and Fennoscandian shields (Vogel *et al.*, 1998, and references therein). Break-up of the late Archaean proto-continent began with continental rifting at ~2·5 Ga (Puchtel *et al.*, 1997). This coincided with the emplacement of numerous 2·4–2·5 Ga mafic–ultramafic layered intrusions (see Fig. 1c). These layered intrusions are found within the Kola craton, in the northern and central parts of the Karelian granite–greenstone terrane (Sharkov *et al.*, 1994; Mitrofanov, 1995), as well as in the Belomorian Mobile Belt (Snyder *et al.*, 1995; Amelin & Semenov, 1996; Higgins *et al.*, 1996; Sharkov *et al.*, 1997; Lobach-Zhuchenko *et al.*, 1998). They vary in composition from lherzolite and olivine gabbronorite to norite, anorthosite and hypersthene diorite (Snyder *et al.*, 1995). Two different magma series are recognized: a siliceous high-Mg, low-Ti basalt and a high-Al, more Fe-rich tholeiitic basalt (Alapieti *et al.*, 1990; Amelin & Semenov, 1996). The parental magmas for most of the layered intrusions are believed to have been generated in a mantle plume (Amelin & Semenov, 1996; Sharkov *et al.*, 1999), and this event is considered to have resulted in a substantial addition of juvenile mantle-derived material to the existing Archaean continent in the Baltic Shield (Puchtel *et al.*, 1997).

Heaman (1997) observed that magmatic rocks of similar age and composition occur in locations as widely spread as Scotland, Greenland, Canada and Wyoming, USA, as well as in the Baltic Shield (Karelia, Finland and Russia). He suggested that these rocks may all have been part of a voluminous mafic magmatic event that marked the break-up of the Late Archaean supercontinent, and may thus be one of the earliest recognized large igneous provinces. A second plume event—which began at ~2 Ga and gave rise to basalts, picrites and komatiites of the Onega plateau, the Pechenga–Imandra belt and the Karsjok–Kittila belt—has been postulated for the region by Puchtel *et al.* (1998).

This complex and extended history of Palaeoproterozoic mafic magmatism was followed by the Svecofennian Orogeny. Its deformational peak occurred at ~1·85 Ga and was associated with the emplacement of potassic granodiorite–granite intrusions (e.g. the Litsa–

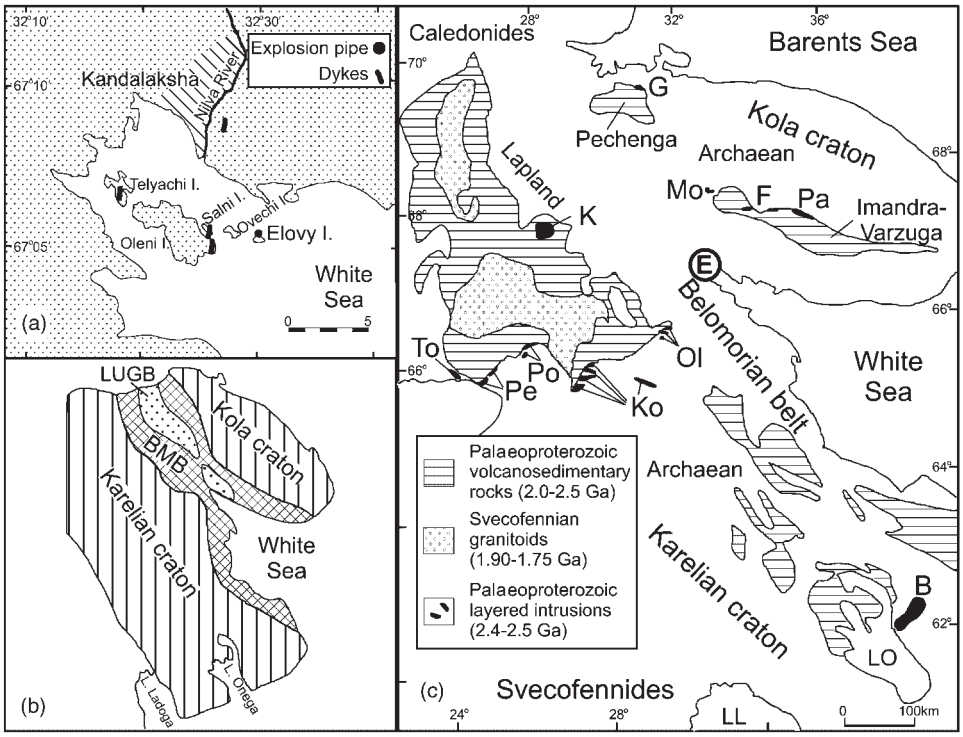

Fig. 1. (a) Map of the Kandalaksha Gulf showing the location of the xenolith-bearing diatremes on Elovy and Salni Islands. (b) Generalized structural relationships of the different crustal domains of the Baltic Shield [adapted from Sharkov *et al.* (1997)]. BMB, Belomorian Mobile Belt; LUGB, Lapland–Umba Granulite Belt. (c) Geological sketch map of the eastern Baltic Shield showing distribution of Palaeoproterozoic rocks and location of xenolith localities [modified from Amelin & Neymark (1998)]. LO, Lake Onega; LL, Lake Ladoga. Palaeoproterozoic layered intrusions are indicated as follows: B, Burakovsky; K, Koitelainen; Ol, Olanga complex; Pe, Penikat; To, Tornia; G, Mt General'skaya; Ko, Koilismaa; Mo, Monch Tundra; Pa, Pana; Po, Portimo; F, Federova Tundra. The Elovy xenolith locality is indicated by the large circled E.

Araguba complex, 1·82–1·72 Ga), lamprophyre dykes (Mitrofanov, 1995), and micaceous pegmatites dated at 1·81–1·75 Ga (Glebovitsky, 1997).

The final phase of magmatic activity within the Baltic Shield is represented by the Devonian lamprophyres that host the xenolith suite (Beard *et al.*, 1996). Approximately 40 such explosion pipes and dykes occur along the southern margin of the Kola Peninsula. They are related to the major alkaline intrusions of Lovozero and Khibina (Kramm *et al.*, 1993).

DESCRIPTION OF SAMPLES

Table 1 gives a brief description of the analysed xenoliths; included are most of the main lithologies observed within the suite. Further details of the petrography have been given by Kempton *et al.* (1995).

The Kola xenolith suite is dominated by mafic garnet granulites that are composed of plagioclase + garnet + clinopyroxene + rutile ± quartz ± phlogopite. *P–T* estimates (Kempton *et al.*, 1995) generally indicate equilibration within the range of granulite facies conditions (750°C, 12–14 kbar). The amount of feldspar is variable, even on a hand-specimen scale, resulting in a banded or gneissic appearance for some samples. Other xenoliths are almost feldspar free (garnet + clinopyroxene + rutile ± plagioclase ± quartz ± phlogopite), and these have been referred to as 'eclogitic' granulites by Kempton *et al.* (1995). On the basis of geochemical arguments, Kempton *et al.* (1995) suggested that these plagioclase-poor rocks are restites after melt extraction from protoliths similar to the more feldspar-rich rocks of the suite. Indeed, the presence of migmatitic granulites (e.g. N41-7 and N57) consisting of siliceous (SiO_2 >63 wt %) quartz + feldspar-rich leucosomes and garnet-rich, feldspar-poor mesosomes provide evidence for just such a partial melting event (Kempton *et al.*, 1995). Some garnet granulites contain metasomatic hornblende or phlogopite (Kempton *et al.* 1995), which can either be pervasive (e.g. 436-11, 435-2E) or confined to bands or veins (e.g. N57). Accessory minerals include apatite, Fe–Ti oxides, scapolite, zircon, sphene and monazite. Chlorite, clays, calcite and analcime are present as alteration phases.

Pyroxenites make up a smaller but significant component of the suite, and are of two types: one is fine grained and contains abundant amphibole (e.g. samples 436-15a and 436-15b), the other is coarse grained and

Table 1: Lithologies and visual estimates of modal mineralogy of analysed xenoliths

Sample	Description	Modes
N27-21	Banded garnet granulite	30% gt, 30% cpx, 30% plag/Kspar, 5% qtz, 5% cc, trace rut, ap, opq
N39	Feldspar-rich garnet granulite	84% plag/Kspar, 10% gt, 5% cpx, 1% cc, trace rut, ap, mt, scap
N41-7	Feldspar + quartz-rich leucosome of migmatitic granulite	60% plag/Kspar, 30% qtz, 5% cpx, 5% gt, trace pyr, cc, rut
N42	Banded garnet granulite	50% cpx, 25% gt, 20% plag, 5% qtz, trace ap, rut
N43	'Eclogitic' granulite	49% cpx, 40% gt, 5% plag, 5% qtz, 1% rut, <1% chlorite, trace ap, cc, zr, monazite
N55	'Eclogitic' granulite	55% cpx, 40% gt, 3% qtz, 2% plag, trace amph, rut, opq, cc
N57M	Mesosome of migmatitic garnet granulite	40% cpx, 30% gt, 25% plag/Kspar, 3% qtz, 1% mica, 1% opq
N57L	Feldspar-rich leucosome of migmatitic garnet granulite	60% plag/Kspar, 20% qtz, 10% gt, 10% cpx, <1% mica, opq
N57Ph	Micaceous band in N57	55% plag, 35% cpx, 8% phlog, 1% opq, <1% gt, trace amph
N61	Garnet granulite	38% cpx, 30% plag, 28% gt, 2% cc, 1% amph, 1% opq
16/89	Garnet granulite	59% plag, 20% gt, 14% cpx, 3% qtz, 3% scap, <1% Kspar, <1% sphene/rut, <1% opq
37-40	Garnet granulite	47% plag, 27% cpx, 23% gt, 3% qtz, <1% opx, <1% amph
37-3(4)	Garnet granulite	35% cpx, 25% pseudomorphs (opx), 20% gt, 15% plag, 3% qtz, 2% rutile, trace amph
67-12	Garnet granulite	40% cpx, 39% gt (largely replaced by kelyphite), 20% plag, 1% sphene, trace amph
435-1	Garnet granulite with amphibole vein	38% plag, 21% gt, 18% cpx, 10% pseudomorphs after opx(?), 6% amph, 4% scap, 3% qtz, trace ap, rut, mica, cc, opq
435-2E	Micaceous 'eclogitic' granulite part of composite xenolith 435-2	35% gt, 32% mica, 25% cpx, 3% pseudomorphs after opx(?), 2% plag, 2% qtz, 1% ap, <1% rut
435-2P	Pyroxenite part of composite xenolith 435-2	95% cpx, 3% amph, 2% pseudomorphs after opx(?), trace opq, rut, mica
435-2B	Micaceous boundary between 435-2E and 435-2P	similar to 435-2P, but with ~2% mica
436-11	Phlogopite–garnet–orthopyroxene rock	45% phlog, 35% gt, 20% opx, trace opq
436-15a	Amphibole pyroxenite	55% cpx, 40% amph, 5% opq, trace cc, analcime
436-15b	Amphibole pyroxenite	49% cpx, 49% amph, <1% cc, <1% analcime, trace ap, pyr, barite, cc
436-24b	Orthopyroxenite	97% opx, 2% interstitial cpx, 1% Kspar
436-25	'Eclogitic' granulite	cpx, gar, opx, rt, ilm, pyrite, clay (precise modes not available)
436-30b	'Eclogitic' granulite	53% cpx, 40% gt, 5% plag, 1% cc, 1% analcime, trace rut, ap, mica

Sample N41-7 is equivalent to sample N41L of Kempton *et al.* (1995). This relatively large xenolith was cut into multiple slabs, and the one analysed here is slab 7. It should be noted also that the modal composition of N41L was reported incorrectly by Kempton *et al.* (1995); values reported here for N41-7 are the correct ones. Modes for 67-12, 37-3(4), 37-40 and 16/89 differ from those of Neymark *et al.* (1993*b*), being visual estimates intended to reflect the primary mineralogy (i.e. kelyphite is included with garnet, etc). Garnet granulites with <5% plagioclase are referred to as 'eclogitic'. Abbreviations: gt, garnet; cpx, clinopyroxene; plag, plagioclase; Kspar, potassium feldspar; qtz, quartz; cc, calcite; rut, rutile; opq, opaque; phlog, phlogopite; amph, amphibole; opx, orthopyroxene; ap, apatite; scap, scapolite; ilm, ilmenite.

nearly amphibole free (e.g. 435-2P). Xenoliths composed largely of hornblende are also present, and these yield Ar–Ar ages of 394 ± 2 Ma (Beard *et al.*, 1996).

Several of the xenoliths are composite in nature. For example, sample 435-2 consists of a mica-rich, plagioclase-poor granulite crosscut by a coarse-grained pyroxenite vein. Similarly, sample N57 is a migmatitic granulite that includes a fine-grained layer of contrasting mineralogy (mica-rich) oriented oblique to the banding of the migmatite (Kempton *et al.*, 1995).

Upper-crustal xenoliths similar to the local Belomorian granite gneisses are present in the Elovy pipe, but ultramafic peridotites have not been found. However, peridotite xenoliths do occur in the kimberlites at Arkangelsk and in a nearby Devonian monticellite kimberlite (A. Beard, personal communication, 1999).

ANALYTICAL PROCEDURES

Rare earth elements

Rare earth element (REE) analyses for most samples were obtained on whole-rock powders of the xenoliths using a Philips PV8060 ICP-AES simultaneous/sequential spectrometer at Royal Holloway, University of London (Table 2). Samples (~0·5 g) were dissolved in HF and $HClO_4$, and the insoluble residues ignited and fused with NaOH. The solutions were passed through ion exchange columns, which separated the REE before analysis. The pyroxenitic portion of sample 435-2 was analysed in duplicate. Samples 16/89, 37-40, 37-3(4) and 67-12 were analysed at IGEM, Moscow, by thermal ionization mass spectrometry (TIMS) isotope dilution techniques using methods described by Puchtel *et al.* (1996). The accuracy and precision of REE determinations are ~ ±3% for La and Lu, and better than ±2% for the other REE.

Sm–Nd, Rb–Sr and U–Pb isotopes

Sm–Nd and Rb–Sr (Table 3) and Pb isotope compositions (Table 4) for whole rocks and some feldspars for samples 16/89, 37-40, 37-3(4) and 67-12 were analysed at the Institute of Precambrian Geology and Geochronology, St Petersburg, using techniques described by Neymark *et al.* (1993*a*, 1994). The isotopic analyses were performed on a MAT-261 eight-collector mass spectrometer in static mode. Procedural blanks during the course of analysis were less than 200 pg for Sm, 100 pg for Nd, 70 pg for Rb, 800 pg for Sr and 5 ± 2 ng for Pb. The remaining U–Th–Pb data in Table 4 were obtained at the USGS laboratory in Denver. Hand-picked mineral separates were sequentially leached for half an hour in 7N HNO_3, 6·5N HCl and rinsed in H_2O on a hotplate. Each stage of the leaching procedure was followed by ultrasonic cleansing for 10–15 min, and the combined leachate solutions were retained for analysis. Pb was purified using the HBr ion-exchange techniques modified from Manhes *et al.* (1978). U–Th–Pb isotope analyses of all minerals were carried out on a VG-54E mass spectrometer equipped with an analogue Daly detector.

Sr, Nd and Pb isotope ratios for the remaining samples were determined at the NERC Isotope Geosciences Laboratory (NIGL) (Tables 3 and 5). Details of the chemical preparation procedures used at NIGL have been given by Kempton (1995) and Royse *et al.* (1998). Two granulite xenoliths (N39 and N41) were leached in 6M HCl on a hot plate for ~1 h; leached and unleached fractions of these samples were analysed for comparison. Sr and Pb were run as the metal species on single Ta and single Re filaments, respectively, using a Finnigan MAT 262 multicollector mass spectrometer in static mode. The samples were spiked using a mixed Sm–Nd spike, and concentrations of Sm and Nd were determined. Nd was run as the metal species on triple Ta–Re–Ta filaments on a VG-354 multicollector mass spectrometer in dynamic mode. Blanks for Sr, Nd and Pb were <1·3 ng, <150 pg and <300 pg, respectively. The effects of fractionation during runs were eliminated by normalizing $^{86}Sr/^{88}Sr$ to 0·1194; $^{146}Nd/^{144}Nd$ was normalized to a value of 0·7219. Sample values for Sr are reported relative to an accepted $^{87}Sr/^{86}Sr$ value for NBS 987 of 0·71024; Nd values are reported relative to a J&M $^{143}Nd/^{144}Nd$ of 0·511125, which is equivalent to a $^{143}Nd/^{144}Nd$ of 0·51186 for La Jolla. Pb isotope ratios have been corrected relative to the average standard Pb isotope compositions of Todt *et al.* (1984). On the basis of repeated runs of NBS 981, the reproducibility of whole-rock Pb isotope measurements made at NIGL (Table 5) is better than ±0·1% per a.m.u.

U, Th and Pb contents of selected whole-rock xenoliths were determined using an isotope dilution–inductively coupled plasma mass spectrometry (ID-ICPMS) technique (Table 5). Weighed amounts of whole-rock powders were spiked using a mixed U–Pb spike and digested in HF and HNO_3; Th was not spiked. Teflon distilled reagents were used throughout the procedure. After evaporation, the samples were taken up in dilute HNO_3 and analysed for ^{204}Pb, ^{208}Pb, ^{232}Th, ^{237}U and ^{235}U by ICPMS at the NERC ICPMS facility, Silwood Park.

The reported analytical uncertainties used in the regression calculations were 0·3% for $^{147}Sm/^{144}Nd$ and 0·005% for $^{143}Nd/^{144}Nd$, the 2σ value for the BCR-1 standard, corresponding to its external reproducibility. To calculate the age, the $^{207}Pb/^{204}Pb$ vs $^{206}Pb/^{204}Pb$ data were regressed using the ISOPLOT/Ex program (Ludwig, 1998), assuming an error correlation coefficient of 0·9. The reported errors for whole rock and mineral separates from samples 16/89, 37-40 and 37-3(4) (Table

Table 2: REE concentrations in selected lower-crustal xenoliths from Elovy Island, Kola Peninsula

	N27-21	N39	N41-7	N42	N43	N55	N57-2L	N57-2M	N57-2Ph	N61	16/89	37-40
La	30·77	12·10	22·40	13·32	33·50	8·92	26·25	24·16	32·97	21·25	19·11	27·39
Ce	69·20	25·75	33·81	28·93	82·63	24·15	43·58	58·06	65·44	52·38	40·51	56·05
Pr	8·46	2·93	3·43	3·43	10·78	3·38	5·01	7·61	7·80	6·78		
Nd	35·30	12·10	11·95	14·70	46·50	15·60	19·43	32·57	29·97	31·50	20·61	28·02
Sm	6·52	2·36	1·89	3·07	8·76	3·30	3·45	6·76	5·14	6·06	4·39	4·917
Eu	1·71	1·00	0·83	0·86	2·22	0·98	0·97	1·70	1·33	1·77	1·491	1·662
Gd	5·57	2·28	1·88	3·23	7·52	3·58	3·10	6·53	3·93	5·35	4·435	3·693
Dy	4·96	2·44	1·99	3·56	6·60	3·92	3·23	6·83	3·56	4·50	4·208	2·505
Ho	0·87	0·44	0·37	0·65	1·17	0·73	0·60	1·25	0·63	0·79		
Er	2·39	1·31	1·11	1·89	3·17	2·07	1·81	3·71	1·76	2·08	2·366	1·255
Yb	1·99	1·15	1·05	1·66	2·87	1·88	1·69	3·44	1·79	1·79	2·151	1·09
Lu	0·32	0·19	0·18	0·27	0·47	0·30	0·28	0·57	0·32	0·30	0·3171	0·163
La/Yb	15·46	10·52	21·33	8·02	11·67	4·74	15·53	7·02	18·42	11·87	8·88	25·13
Eu/Eu*	0·87	1·32	1·35	0·84	0·84	0·87	0·91	0·78	0·91	0·95	1·03	1·19

	37-3(4)	435-1	435-2E	435-2P	435-2B	436-11	436-15a	436-15b	436-24b	436-25	436-30b
La	11·28	35·75	12·39	13·95	16·85	10·15	24·41	21·87	8·02	25·82	18·55
Ce	27·28	76·17	26·94	48·09	58·08	19·18	58·97	74·51	16·42	55·69	43·67
Pr		8·75	3·60	7·65	8·98	2·22	7·45	10·94	1·91	6·29	5·27
Nd	14·64	33·70	16·21	37·22	40·60	9·90	30·10	49·90	6·40	23·80	22·00
Sm	3·199	5·47	3·59	7·64	8·60	2·83	5·44	9·47	1·26	4·18	4·23
Eu	0·9486	1·63	1·10	1·80	1·97	0·52	1·45	2·63	0·32	1·21	1·09
Gd	3·254	4·17	3·95	5·91	6·73	3·60	4·26	7·58	1·05	3·64	3·82
Dy	3·215	3·44	4·76	4·28	4·62	4·87	3·27	5·57	0·81	3·33	3·68
Ho		0·61	0·89	0·64	0·68	0·91	0·54	0·92	0·17	0·59	0·68
Er	1·873	1·67	2·54	1·32	1·50	2·73	1·33	2·24	0·42	1·61	1·94
Yb	1·743	1·50	2·40	0·85	0·84	2·45	1·00	1·70	0·35	1·35	1·70
Lu	0·2572	0·25	0·40	0·11	0·11	0·42	0·16	0·27	0·06	0·22	0·28
La/Yb	6·47	23·83	5·16	16·41	20·06	4·14	24·41	12·86	22·91	19·13	10·91
Eu/Eu*	0·90	1·05	0·89	0·83	0·79	0·50	0·92	0·95	0·85	0·95	0·83

Samples 16/89, 37-3(4) and 37-40 were analysed by isotope dilution (IGEM); remaining samples were analysed by ICP-AES (Royal Holloway, University of London).

Table 3: Sr and Nd isotope data for Kola granulite and pyroxenite xenoliths

Sample		Rb	Sr	$^{87}Rb/^{86}Sr$	$^{87}Sr/^{86}Sr$	Sm	Nd	$^{147}Sm/^{144}Nd$	$^{143}Nd/^{144}Nd$	ε_{Nd} (0)	ε_{Nd} (1·5 Ga)	ε_{Nd} (2·4 Ga)	T_{DM} (t_1 = 1·5 Ga)
Granulite xenoliths													
N27-21	WR	24·9	628·0	0·1147	0·70941	6·61	34·73	0·1151	0·511456	−23·1	−7·4	2·1	2·49
	WR rpt				0·70951	6·53	34·50	0·1144	0·511434	−23·5	−7·7	1·9	2·51
N39	WR UL	29·8	680·6	0·1267	0·70886	2·49	12·06	0·1245	0·511620	−19·9	−6·0	2·4	2·40
	WR L				0·70808				0·511781				
	WR LL				0·71200				0·511564				
N41-7	WR UL	10·9	599·9	0·0526	0·71229	2·00	11·80	0·1026	0·511411	−24·0	−5·9	5·1	2·39
	WR L				0·71222				0·511643				
N42	WR	5·6	163·3	0·0993	0·71183	2·99	13·50	0·1340	0·511477	−22·7	−10·7	−3·4	2·70
N43	WR	9·7	183·1	0·1532	0·70521	8·57	44·48	0·1165	0·511261	−26·9	−11·5	−2·2	2·75
N55	WR	9	131·2	0·1984	0·70669	3·23	13·81	0·1415	0·511653	−19·3	−8·7	−2·2	2·58
N57-2M	WR	14	373·4	0·1085	0·71003	7·01	33·15	0·1278	0·511575	−20·8	−7·6	0·5	2·50
N57-2Ph	WR				0·71005	5·37	29·87	0·1087	0·512095	−10·6	6·3	16·6	1·44
N57-2L	WR	10·8	430·3	0·0726	0·71196	3·66	20·06	0·1102	0·511498	−22·3	−5·7	4·5	2·38
N61	WR	20·8	557·1	0·1080	0·70619	5·87	28·76	0·1234	0·511922	−14·0	0·1	8·7	1·96
16/89*	WR	20·66	672·2	0·0889	0·70755	4·771	22·09	0·1305	0·511680	−18·6	−6·0	1·7	2·40
	Pl	6·437	497·66	0·0374	0·70519	0·204	2	0·0617	0·511024	−31·4	−5·6	10·2	2·37
	Kspar	124·9	2481·7	0·1456	0·70710	0·361	3·013	0·0724	0·511202	−28·0	−4·1	10·4	2·27
	Cpx	1·334	40·801	0·0946	0·70543	8·26	36·43	0·1370	0·511529	−21·6	−10·2	−3·3	2·67
	Gar	2·279	3·003	2·1985	0·71797	3·43	2·905	0·7137	0·517436	93·6	−6·0	−66·7	2·39
	Ap	0·707	911·98	0·0022	0·70512	73·15	443·2	0·0998	0·511139	−29·2	−10·7	0·6	2·70
37-40*	WR	14·76	1143·1	0·0374	0·70526	5·566	30·9	0·1089	0·511316	−25·7	−9·0	1·3	2·59
	Cpx	2·229	181·33	0·0356	0·70520	4·94	24·13	0·1238	0·511286	−26·3	−12·4	−3·9	2·81
	Gar	0·79	3·399	0·6731	0·71424	4·11	3·56	0·6979	0·517173	88·5	−8·1	−66·9	2·53
	Pl	12·94	1625·9	0·0230	0·70403	0·38	3·704	0·0621	0·510800	−35·8	−10·0	5·7	2·66
37-3(4)*	WR	17·73	127·7	0·4021	0·71855	3·004	13·81	0·1315	0·511546	−21·3	−8·8	−1·2	2·59
	Gar-1	—	—	—	—	2·376	1·931	0·7437	0·517773	100·2	−5·3	−69·4	2·34
	Gar-2	—	—	—	0·71468	1·678	1·308	0·7751	0·517898	102·6	−9·0	−76·8	2·58
	Pl	6·659	269	0·0717	0·71673	0·369	3·386	0·0658	0·511037	−31·2	−6·1	9·2	2·41
	Cpx	4·458	22·127	0·5834	0·71387	4·695	23·36	0·1215	0·511343	−25·2	−10·9	−2·1	2·71
67-12*	WR	18·79	313·4	0·1735	0·71022	8·447	49·48	0·1032	0·511404	−24·0	−6·1	4·8	2·41
435-1	WR	12·6	768·5	0·0474	0·70583	5·33	32·99	0·0977	0·511531	−21·6	−2·6	9·0	2·16
435-2E	WR	62·3	368·0	0·4902	0·71676	4·07	16·64	0·1479	0·511939	−13·7	−4·3	1·4	2·28

Table 3: continued

Sample		Rb	Sr	$^{87}Rb/^{86}Sr$	$^{87}Sr/^{86}Sr$	Sm	Nd	$^{147}Sm/^{144}Nd$	$^{143}Nd/^{144}Nd$	ε_{Nd} (0)	ε_{Nd} (1·5 Ga)	ε_{Nd} (2·4 Ga)	T_{DM} (t_1 = 1·5 Ga)
436-11	WR	74·6	24·5	9·0253	0·95638	2·69	8·18	0·1990	0·512317	−6·3	−6·8	−7·1	2·45
436-30b	WR	8·2	391·5	0·0606	0·70885	3·76	19·16	0·1186	0·511612	−20·0	−5·1	4·1	2·33
436-30b	WR rpt				0·70883	4·10	21·04	0·1177	0·511590	−20·5	−5·3	3·9	2·35
Pyroxenite xenoliths													
435-2B	WR	4·2	118·4	0·1026	0·70947	8·25	39·11	0·1274	0·511641	−19·5	−6·5	1·3	2·44
435-2P	WR	1·8	88·7	0·0587	0·70864	8·11	37·92	0·1292	0·511634	−19·6	−6·3	1·8	2·42
436-15a	WR	5·1	85·8	0·1719	0·70557	9·30	48·20	0·1166	0·512290	−6·8	8·6	18·0	1·23
436-15a	WR rpt				0·70555				0·512288				
436-15b	WR	12·3	680·2	0·0523	0·70694	5·26	28·84	0·1103	0·512250	−7·6	9·1	19·2	1·18
436-15b	WR rpt				0·70692				0·512243				
436-24b	WR	5·1	85·6	0·1720	0·70789	1·01	5·91	0·1038	0·512345	−5·8	12·2	23·1	0·85

*Analyses performed at IPGG, St Petersburg. All other analyses performed at NIGL.
WR, whole rock; WR rpt, a whole-rock repeat analysis on a new sample dissolution; UL, unleached; L, leached; LL, leachate; cpx, clinopyroxene; pl, plagioclase; Kspar, potassium feldspar; gar, garnet; ap, apatite. Rb, Sr, Sm and Nd concentrations in ppm. (See text for discussion of model age calculations.)

Table 4: U–Th–Pb isotope data for minerals and whole rocks from Kola lower-crustal xenoliths

Sample	Rock/ mineral	Sample wt (mg)	U	Th	Pb	$^{206}Pb/^{204}Pb$*	2σ (%)	$^{207}Pb/^{204}Pb$*	2σ (%)	$^{208}Pb/^{204}Pb$*	2σ (%)	$^{238}U/^{204}Pb$	Th/U
Granulite xenoliths													
37-40†	WR	241·9	0·518	—	8·76	15·515	0·10	14·993	0·15	36·479	0·20	3·47	—
37-40	WR	73·51	0·541	1·41	—	—	—	—	—	—	—	—	2·6
37-40†	Pl	>50	—	—	—	14·334	0·10	14·809	0·15	34·425	0·20	—	—
37-40†	Pl (leach)	—	—	—	—	17·126	0·10	15·239	0·15	40·158	0·20	—	—
37-40	Pl(1)	2·24	0·016	0·034	12·3	14·606	0·15	14·965	0·18	34·759	0·23	0·07	2·13
37-40	Pl(1) (leach)	—	(0·028)‡	(0·098)	(0·808)	17·282	0·71	15·300	0·40	38·325	0·37	2·12	3·57
37-40	Gar	75·94	0·0035	0·0142	0·022	19·551	0·15	15·716	0·20	42·296	0·38	10·55	4·09
37-40	Gar (leach)		(0·337)	(0·752)	(78·46)	17·882	0·12	15·546	0·18	38·135	0·23	0·27	2·23
37-40	Cpx	7·36	0·025	0·056	0·605	14·190	0·42	14·783	0·28	34·204	0·33	2·28	2·26
16/89†	WR	207·59	0·283	—	7·66	16·886	0·10	15·373	0·15	38·220	0·20	2·28	—
16/89	WR	60·2	0·252	0·844	—	—	—	—	—	—	—	—	3·35
16/89†	Pl	>50	—	—	—	15·417	0·10	15·213	0·15	35·398	0·20	—	—
16/89†	Pl (leach)	—	—	—	—	17·898	0·10	15·480	0·15	40·496	0·20	—	—
16/89†	Kspar	>50	—	—	—	15·491	0·10	15·302	0·15	35·206	0·20	—	—
16/89†	Kspar (leach)	—	—	—	—	16·572	0·10	15·378	0·15	37·488	0·20	—	—
16/89	Pl(1)	4·95	0·0037	0·0080	3·33	15·289	0·10	15·180	0·15	35·290	0·20	0·06	2·17
16/89	Pl(1) (leach)	—	(0·019)	(0·073)	(32·4)	19·952	0·10	15·823	0·15	39·190	0·21	0·04	3·84
16/89	Ap	9·73	0·483	3·01	3·61	17·260	0·19	15·429	0·26	39·078	0·27	8·42	6·23
16/89	Ru	3·41	4·18	3·36	2·59	39·091	0·35	16·624	0·22	49·327	0·31	138	0·81
16/89	Gar	53·5	0·0071	0·083	0·030	19·716	0·18	15·679	0·20	41·948	0·36	16	11·69
16/89	Gar (leach)	—	(2·50)	(6·67)	(648)	19·351	0·16	15·799	0·24	38·757	0·27	0·25	2·67
16/89	Cpx	8·53	0·024	0·328	0·721	17·167	0·16	15·466	0·19	39·731	0·24	2·07	13·97
16/89	Cpx (leach)	—	(0·046)	(0·259)	(4·07)	18·261	0·21	15·601	0·25	38·594	0·27	0·72	5·6
37-3(4)†	WR	223·3	0·179	—	4·60	16·448	0·10	15·440	0·15	37·108	0·20	2·35	—
37-3(4)	WR	113·19	0·067	0·239	—	—	—	—	—	—	—	—	3·59
37-3(4)†	Pl	>50	—	—	—	15·713	0·10	15·405	0·15	35·694	0·20	—	—
37-3(4)†	Pl (leach)	—	—	—	—	18·002	0·10	15·539	0·15	40·588	0·20	—	—
37-3(4)	Pl(1)	4·52	0·0080	0·020	6·09	15·487	0·14	15·390	0·17	35·276	0·22	0·08	2·53
37-3(4)	Pl(1) (leach)	—	(1·20)	(0·319)	(2·04)	18·303	0·21	15·597	0·22	37·729	0·25	37·74	0·27
37-3(4)	Gar	59·64	0·0043	0·014	0·047	19·642	0·24	15·714	0·27	40·591	0·31	6·14	3·25
37-3(4)	Gar(1)	74·62	0·0025	0·013	0·019	19·264	1·30	15·624	1·30	41·596	1·40	8·99	5·06
37-3(4)	Gar(1) (leach)	—	(0·224)	(0·932)	(42·4)	17·964	0·12	15·566	0·17	38·233	0·22	0·33	4·15
37-3(4)	Cpx	8·18	0·021	0·326	0·824	17·731	0·16	15·585	0·19	39·505	0·24	1·61	15·69
37-3(4)	Cpx (leach)	—	(0·189)	(1·64)	(17·0)	18·090	0·17	15·594	0·20	38·555	0·24	0·70	88·65
Host ultramafic lamprophyre													
37-42†	WR	120·23	2·10	—	8·50	19·327	0·10	15·561	0·15	41·984	0·20	16·6	—
37-42	WR	23·93	2·10	7·80	—	—	—	—	—	—	—	—	3·72

*Isotope ratios corrected for spike contributions, procedural blank and mass discrimination.
†Analyses performed at IPGG, St Petersburg. All other analyses carried out at the USGS in Denver.
‡Values for leaches in parentheses represent total amount of leached element in ng.
WR, whole rock; Pl, plagioclase; Gar, garnet; Cpx, clinopyroxene; Kspar, potassium feldspar; Ap, apatite; Ru, rutile.

Table 5: U–Th–Pb isotope data for whole-rock Kola granulite and pyroxenite xenoliths

Sample	U	Th	Pb	$^{206}Pb/^{204}Pb$	$^{207}Pb/^{204}Pb$	$^{208}Pb/^{204}Pb$	$^{238}U/^{204}Pb$	Th/U
Granulite xenoliths								
N27-21				17·497	15·520	39·792		
N39	0·25	0·62	5·14	17·192	15·312	39·534	3·07	2·48
N39 (L)				16·680	15·255	38·319		
N39 (LL)				19·240	15·589	44·411		
N41-7	0·29	0·88	12·12	18·222	15·638	41·273	1·57	3·03
N41-7 (L)				17·496	15·551	39·358		
N42	0·16	0·91	8·16	19·827	15·771	45·790	1·40	5·69
N43	0·09	0·18	3·32	19·450	15·582	44·832	1·89	2·00
N55	0·09	0·24	7·66	19·359	15·656	44·826	0·82	2·67
N57-2M	0·28	0·95	9·31	18·085	15·629	40·487	1·95	3·39
N57-2Ph	2·93	11·11	19·01	19·034	15·674	40·748	10·19	3·79
N57-2L				17·293	15·594	38·617		
N61				18·793	15·574	42·731		
16/89	0·283		7·66	16·886	15·373	38·220	2·28	
37-40	0·518		8·76	15·515	14·993	36·490	3·47	
37-3(4)	0·179		4·6	16·448	15·440	37·108	2·35	
67-12				18·563	15·618	38·880		
435-1	0·54	1·62	9·56	17·999	15·501	40·811	3·68	3·00
435-2E	0·22	0·29	4·83	17·706	15·527	39·626	2·91	1·32
436-11	0·25	2·23	1·49	22·474	16·027	54·825	13·68	8·92
436-30b				18·545	15·503	37·457		
436-30b				18·518	15·469	37·369		
Pyroxenite xenoliths								
435-2P	0·14	0·57	1·88	19·066	15·625	43·239	5·08	4·07
435-2B				19·199	15·653	43·690		
436-15a				17·391	15·424	36·840		
436-15a				17·387	15·421	36·808		
436-15b	0·85	1·93	4·38	17·954	15·421	37·788	12·10	2·27
436-24b				17·557	15·587	37·991		

U, Th and Pb concentrations in ppm. (L), samples leached in 6M HCl; (LL), leachate; remaining samples unleached. Data for sample 67-12 from Neymark *et al.* (1993*b*).

4) were calculated using the Ludwig PBDAT program; the errors were propagated to include uncertainties of blanks, spike subtraction and mass-discrimination.

Ar–Ar dating

Ultraviolet (UV) $^{40}Ar/^{39}Ar$ laser analysis was carried out on four ~1 mm phlogopite grains that were selected from a crushed and cleaned separate of sample 436-11. They were fast neutron irradiated for 5 h at the Risø nuclear reactor in Denmark. The irradiation time of 5 h was not optimized for samples of this age, resulting in low Ar yields and higher than normal errors. The grains were loaded into an ultra-high vacuum laser port with an UV-grade fused silica window and baked to 120°C overnight using an IR heat lamp to remove absorbed atmospheric argon from the samples and laser port walls.

A pulsed quadrupled Spectron SL401 Nd–YAG UV laser (λ = 266 nm) with a pulse length of 10 ns and repetition rate of 10 Hz and a beam diameter of ~20 μm was rastered over 50 and 100 μm squares for 8 min. A Märzhäuser MAC 4000 computerized X–Y–Z stage, attached to a customized Leica DMR microscope, was used to control the raster speed (20 μm/s) and the size of the laser pit. For higher spatial resolution profiling, a step scanning technique was used. The X–Y–Z stage was programmed to raster a traverse 450–630 μm long, with a 20 μm wide beam starting at the edge of the grain.

Subsequent analyses progressed inwards towards the centre of the grain.

The Ar isotopes released after each laser ablation were cleaned using three Zr–Al getters and analysed using a high-sensitivity mass spectrometer (MAP 215-50) with a Johnston multiplier detector. Further details regarding the mass spectrometer and the UV laser technique have been given by Kelley *et al.* (1994), Arnaud & Kelley (1997) and Wartho *et al.* (1999). A J value of 0·003564 $\pm$ 0·000018 was calculated for the irradiated sample based on the analysis of biotite standard GA1550 (97·9 Ma, McDougall & Harrison, 1988). Corrections were made for blanks (1×10^{-11}, 6×10^{-15}, 3×10^{-14}, 6×10^{-14} and 1×10^{-13} cm^3 STP for ^{40}Ar, ^{39}Ar, ^{38}Ar, ^{37}Ar and ^{36}Ar, respectively), mass spectrometer and reactor interferences. ^{40}Ar/^{39}Ar UV laser analyses are given in Table 6.

RESULTS

Major and trace element variations with MgO

Major element variations within the Kola xenolith suite have been studied in detail by Kempton *et al.* (1995). This work showed that the protoliths of the granulites ranged in composition from gabbro to tonalite, and that most of the xenoliths can be interpreted as a cogenetic suite of igneous rocks of tholeiitic affinity related by olivine fractionation. The major element compositions of five previously unreported samples (for which new isotope data are also reported here) are listed in Table 7, along with new trace element data for samples 436-24b and 436-25. These new data overlap the range of compositions previously reported and support the petrogenetic interpretations of Kempton *et al.* (1995). The full major and trace element dataset for the Kola xenolith suite can be obtained from the *Journal of Petrology* Web site (http://www.petrology.oupjournals.org).

It has recently been suggested that the Kola lower-crustal xenoliths may be synchronous with, and perhaps genetically related to, the 2·4–2·5 Ga mafic magmatism of the northern Baltic Shield (Sharkov *et al.*, 1999). We have therefore compared the compositions of the xenoliths with data for Palaeoproterozoic volcanic (Fig. 2a–c) and plutonic rocks (Fig. 2d–f) of the northern Baltic Shield. Included are 2·4 Ga komatiites of the Vetreny Belt (Puchtel *et al.*, 1996; 1997), 2·0 Ga picrites, basalts and evolved volcanic rocks of the Onega plateau (Puchtel *et al.*, 1998) and Pechenga–Varzuga (Sharkov *et al.*, 1997), and 2·4–2·5 Ga mafic layered intrusions from Karelia and the Belomorian Mobile Belt (Sharkov *et al.*, 1994, 1995; Snyder *et al.*, 1995, 1996; Amelin & Semenov, 1996; Higgins *et al.*, 1996; Chistyakov *et al.*, 1997; Lobach-Zhuchenko *et al.*, 1998).

The xenoliths show substantial overlap in composition with both the extrusive and intrusive Palaeoproterozoic rocks for most elements (e.g. SiO_2, Al_2O_3, Fe_2O_3, CaO/Al_2O_3, Ni, Zr/Y vs MgO), although some differences exist:

(1) in the plots of Al_2O_3 vs MgO (Fig. 2a and d), the xenoliths overlap the trend shown by the extrusive rocks, but only rocks from the layered intrusions extend to the high Al_2O_3 contents (>15 wt %) observed for some of the plagioclase-rich Kola xenoliths (e.g. N39, 37-40 and 16/89);

(2) in the plots of SiO_2 vs MgO (Fig. 2b and e) the siliceous leucosomes of N41-7 and N57 are most similar to evolved extrusive rocks;

(3) the unusual mineralogy of 436-11 (see Table 1) means that it has higher Al_2O_3 and total alkalis (not shown), but lower SiO_2 than would be expected on the basis of its MgO content;

(4) pyroxenites tend to have significantly lower SiO_2 and Al_2O_3 but higher CaO/Al_2O_3 (not shown) at a given MgO than the granulite xenoliths, although some websterites from the Burakovsky layered intrusion have similarly low Al_2O_3 and high CaO/Al_2O_3 for their MgO contents. In contrast, Ni vs MgO systematics for the xenoliths are similar to the trends shown by both extrusive and plutonic Palaeoproterozoic rocks (Fig. 2c and f), consistent with the interpretation that some of the variation observed within the xenolith suite is due to olivine fractionation and/or accumulation in the protoliths (Kempton *et al.*, 1995.)

Trace element variations

The new REE, U, Th and Pb data presented in Tables 2, 4 and 5 are combined with previously published trace element data (Kempton *et al.*, 1995) to construct a series of primitive-mantle-normalized trace element diagrams in Fig. 3. The trace element patterns for the Kola garnet granulite xenoliths are generally similar to one another. Exceptions are typically xenoliths with unusual mineralogies (e.g. 436-24b, 436-11; Table 1) or unusual major element chemical compositions (e.g. N39; Kempton *et al.*, 1995). All are light REE (LREE) enriched and most have small negative Eu anomalies (Eu/Eu* = 0·78–0·95; see Table 2). The granulite xenoliths are also markedly enriched in Pb, but show relative depletions in U, Th, Nb, Ti and P. In comparison with the feldspar-rich garnet granulites (Fig. 3a and c), feldspar-poor 'eclogitic' granulites (Fig. 3b) tend to have lower La/Yb ratios (see Table 2) and, with the exception of the mica-rich samples (Fig. 3d), lower concentrations of the most incompatible elements (e.g. Rb, Ba, Th, U, Nb, K, P). The trace element patterns of samples N42 and 37-3(4) (Fig. 3a) are more similar to those of the feldspar-poor granulites

Table 6: $^{40}Ar/^{39}Ar$ UV laser analyses of phlogopite grains from 436-11

Run	Distance from rim (μm)	±	Age (Ma)	±	$^{40}Ar^*/^{39}Ar$	±	$^{40}Ar/^{39}Ar$	±	$^{38}Ar/^{39}Ar$	±	$^{37}Ar/^{39}Ar$	±	$^{36}Ar/^{39}Ar$	±	^{39}Ar (cm^3)	±
Phlogopite 1																
Rim 100 μm^2	80	50	778·3	18·0	151·35	4·25	147·23	1·58	0·0271	0·0039	0·0331	0·0210	0·0000	0·0000	1·86E − 12	1·85E − 14
Core–rim 100 μm^2	190	50	1507·8	14·9	366·60	5·02	370·53	2·97	0·0100	0·0040	0·0266	0·0212	0·0133	0·0137	1·80E − 12	1·41E − 14
Core–rim 100 μm^2	330	50	1811·0	12·2	485·05	4·57	483·15	2·59	0·0118	0·0038	0·0058	0·0204	0·0000	0·0000	1·91E − 12	9·83E − 15
Core 100 μm^2	480	50	1945·8	11·5	544·45	4·50	546·94	1·94	0·0180	0·0032	0·0000	0·0000	0·0084	0·0137	1·77E − 12	5·90E − 15
520 μm × 20 μm traverse 1a	10	10	788·7	18·0	153·85	4·25	153·35	1·91	0·0310	0·0030	0·0000	0·0000	0·0000	0·0000	1·93E − 12	2·30E − 14
520 μm × 20 μm traverse 1b	30	10	1190·0	14·0	262·06	3·98	260·88	1·44	0·0093	0·0037	0·0484	0·0197	0·0000	0·0000	1·94E − 12	9·83E − 15
520 μm × 20 μm traverse 1c	50	10	1528·6	12·6	374·12	4·16	367·11	1·32	0·0147	0·0039	0·0258	0·0217	0·0000	0·0000	1·86E − 12	5·90E − 15
520 μm × 20 μm traverse 1d	70	10	1606·4	14·4	402·97	5·08	400·26	3·14	0·0123	0·0039	0·0000	0·0000	0·0000	0·0000	1·84E − 12	1·41E − 14
520 μm × 20 μm traverse 1e	90	10	1900·1	13·4	523·79	5·38	526·05	3·86	0·0188	0·0029	0·0010	0·0200	0·0077	0·0127	1·95E − 12	1·41E − 14
520 μm × 20 μm traverse 1f	110	10	1647·1	14·9	418·57	5·38	418·76	3·93	0·0160	0·0028	0·0000	0·0000	0·0007	0·0124	1·99E − 12	1·85E − 14
520 μm × 20 μm traverse 1g	130	10	1733·1	11·6	452·68	4·13	452·22	2·19	0·0242	0·0035	0·0295	0·0193	0·0000	0·0000	2·09E − 12	9·83E − 15
520 μm × 20 μm traverse 1h	160	10	1781·0	17·8	472·43	7·06	475·28	6·33	0·0198	0·0054	0·0444	0·0365	0·0096	0·0108	1·48E − 12	1·97E − 14
520 μm × 20 μm traverse 1i	180	10	1909·7	11·1	528·08	4·18	528·20	2·89	0·0208	0·0056	0·0093	0·0336	0·0004	0·0102	1·62E − 12	8·86E − 15
520 μm × 20 μm traverse 1j	200	10	2020·0	12·3	579·06	5·09	575·14	4·12	0·0232	0·0048	0·0837	0·0376	0·0000	0·0000	1·66E − 12	1·18E − 14
520 μm × 20 μm traverse 1k	220	10	1961·6	13·8	551·70	5·70	554·89	4·98	0·0248	0·0053	0·0087	0·0310	0·0108	0·0095	1·74E − 12	1·56E − 14
520 μm × 20 μm traverse 1l	250	10	2188·8	13·1	663·39	6·01	670·46	5·15	0·0069	0·0051	0·0663	0·0353	0·0239	0·0108	1·54E − 12	1·18E − 14
520 μm × 20 μm traverse 1m	270	10	2227·7	14·7	683·95	7·03	682·46	6·38	0·0203	0·0048	0·0173	0·0332	0·0000	0·0000	1·67E − 12	1·56E − 14
520 μm × 20 μm traverse 1n	290	10	2116·4	12·6	626·24	5·47	629·04	4·94	0·0217	0·0046	0·0000	0·0000	0·0095	0·0080	1·99E − 12	1·56E − 14
Core 50 μm^2	350	25	2046·0	16·2	591·57	7·24	594·49	6·42	0·0106	0·0055	0·0644	0·0377	0·0099	0·0115	1·45E − 12	1·56E − 14
350 μm × 20 μm traverse 2a	10	10	541·5	21·3	98·23	4·44	100·78	0·85	0·0136	0·0081	0·0338	0·0493	0·0086	0·0148	1·13E − 12	8·86E − 15
350 μm × 20 μm traverse 2b	30	10	868·8	18·2	173·57	4·51	174·91	1·83	0·0052	0·0069	0·0413	0·0471	0·0045	0·0140	1·14E − 12	1·18E − 14
350 μm × 20 μm traverse 2c	55	10	1148·6	14·6	249·75	4·11	247·97	2·12	0·0308	0·0065	0·0436	0·0397	0·0000	0·0000	1·40E − 12	1·18E − 14
350 μm × 20 μm traverse 2d	85	10	1391·7	16·3	326·27	5·22	326·42	3·84	0·0219	0·0060	0·0113	0·0409	0·0005	0·0120	1·33E − 12	1·56E − 14

Run	Distance from rim (μm)	±	Age (Ma)	±	$^{40}Ar^*/^{39}Ar$	±	$^{40}Ar/^{39}Ar$	±	$^{38}Ar/^{39}Ar$	±	$^{37}Ar/^{39}Ar$	±	$^{36}Ar/^{39}Ar$	±	^{39}Ar (cm^3)	±
Phlogopite 2																
500 μm × 20 μm traverse 1a	5	10	410·3	164·3	71·65	32·08	83·11	3·31	0·0000	0·0000	0·0000	0·0000	0·0388	0·1081	2·15E – 13	7·25E – 15
500 μm × 20 μm traverse 1b	25	10	412·4	89·9	72·06	17·57	71·49	2·18	0·0000	0·0000	0·0000	0·0000	0·0000	0·0000	3·93E – 13	1·07E – 14
500 μm × 20 μm traverse 1c	45	10	580·9	31·3	106·59	6·69	112·87	0·88	0·0000	0·0000	0·0000	0·0000	0·0212	0·0225	1·03E – 12	7·25E – 15
500 μm × 20 μm traverse 2a	5	10	870·4	23·3	173·97	5·81	172·69	1·54	0·0006	0·0072	0·0169	0·0481	0·0000	0·0000	1·23E – 12	1·07E – 14
Rim 50 μm^2	40	25	602·4	20·9	111·23	4·51	112·02	1·53	0·0359	0·0066	0·0191	0·0372	0·0027	0·0144	1·01E – 12	1·37E – 14
Core–rim 50 μm^2	115	25	697·6	23·6	132·45	5·35	132·01	3·90	0·0181	0·0054	0·0754	0·0323	0·0000	0·0000	1·23E – 12	3·63E – 14
Core–rim 50 μm^2	180	25	1189·6	15·2	261·95	4·39	270·70	2·16	0·0231	0·0057	0·0323	0·0322	0·0296	0·0131	1·16E – 12	9·25E – 15
Core–rim 50 μm^2	250	25	1674·8	15·1	429·36	5·55	433·03	4·52	0·0028	0·0051	0·0000	0·0000	0·0124	0·0110	1·32E – 12	1·37E – 14
Core 50 μm^2	330	25	1786·2	12·1	474·60	4·48	470·40	3·11	0·0126	0·0057	0·0000	0·0000	0·0000	0·0000	1·40E – 12	9·25E – 15
Core 50 μm^2	430	25	1901·3	14·1	524·33	5·71	521·60	3·60	0·0095	0·0057	0·0606	0·0379	0·0000	0·0000	1·55E – 12	1·07E – 14
Core 50 μm^2	505	25	1810·6	12·6	484·86	4·74	486·49	3·45	0·0064	0·0061	0·0042	0·0285	0·0055	0·0110	1·32E – 12	9·25E – 15
Phlogopite 3																
450 μm × 20 μm traverse 1a	10	5	740·8	34·6	142·46	8·08	163·86	2·81	0·0589	0·0114	0·2569	0·0561	0·0724	0·0261	1·12E – 12	1·90E – 14
630 μm × 20 μm traverse 2a	20	5	717·8	14·7	137·11	3·33	140·74	1·00	0·0090	0·0046	0·0139	0·0274	0·0123	0·0108	2·15E – 12	1·47E – 14
Core 50 μm^2	520	25	1756·1	23·6	462·12	9·41	468·89	8·43	0·0000	0·0000	0·0000	0·0000	0·0229	0·0150	1·55E – 12	2·78E – 14
Core 50 μm^2	620	25	1704·1	14·2	440·98	5·21	439·91	2·22	0·0000	0·0000	0·0237	0·0401	0·0000	0·0000	1·46E – 12	7·25E – 15
Phlogopite 4																
550 μm × 20 μm traverse 1a	10	10	697·9	48·7	132·52	11·14	137·78	1·71	0·0319	0·0163	0·2611	0·0940	0·0178	0·0373	4·08E – 13	4·89E – 15
Core 50 μm^2	325	25	1542·1	16·1	379·04	5·55	379·70	4·30	0·0000	0·0000	0·0196	0·0315	0·0022	0·0119	1·22E – 12	1·37E – 14
Core 50 μm^2	380	25	1557·9	15·3	384·84	5·31	384·72	3·91	0·0000	0·0000	0·0000	0·0000	0·0000	0·0000	1·87E – 12	1·90E – 14

Phlogopite 1 grain is 1·2 mm × 1·0 mm; Phlogopite 2 grain is 0·85 mm × 1·2 mm; Phlogopite 3 grain is 1·1 mm × 0·85 mm; Phlogopite 4 grain is 1·4 mm × 0·9 mm. Age range of rim analyses is 410·3 ± 164·3 to 788·7 ± 18·0 Ma. Unweighted mean of rim analyses (n = 7) is 615·6 ± 147·3 Ma. Age range of core analyses is 1542·1 ± 16·1 to 2227·7 ± 14·7 Ma. Unweighted mean of oldest line traverse core analyses (n = 5) is 2102·9 ± 100·0 Ma. $^{40}Ar^*$ is radiogenic argon, i.e. $^{40}Ar^* = {}^{40}Ar(total) - {}^{40}Ar(atmospheric)$.

Table 7: Whole-rock major element compositions of granulite xenoliths from Kola

	Xenolith						Host rock
Sample:	67-12	37-40	16/89	37-3(4)	436-24b	436-25	37-42
SiO_2	52·95	51·45	49·93	51·92	50·69	44·69	37·30
TiO_2	1·21	0·71	1·08	0·72	0·26	0·83	2·19
Al_2O_3	13·53	18·06	18·46	14·89	4·68	11·62	7·78
Fe_2O_3	1·43	3·40	3·10	1·91	15·02	12·47	3·25
FeO	7·44	4·46	5·63	6·92			4·62
MnO	0·10	0·13	0·15	0·16	0·19	0·17	0·13
MgO	7·29	3·97	4·02	7·25	24·45	12·50	8·41
CaO	7·57	7·15	8·82	8·80	1·98	11·90	13·25
Na_2O	3·08	5·67	4·01	3·87	0·70	2·13	3·57
K_2O	1·06	0·99	1·29	0·90	0·24	0·47	1·61
P_2O_5	0·37	0·38	0·18	0·11	0·04	0·30	0·45
LOI	3·77	3·15	2·28	2·04	1·28	2·58	16·12
Sum	99·82	99·56	99·97	99·50	99·53	99·66	99·96
Nb					6	19	
Zr					27	59	
Y					5	17	
Sr					86	340	
Rb					5	9	
Ba					300	247	
Zn					231	107	
Cu					15	553	
V					107	245	
Sc					16	40	
Ni					1047	280	
Cr					6380	1110	

(Fig. 3b), which may be due to the fact that these samples have the lowest modal abundance of plagioclase of the feldspar-rich granulites (Table 1). Sample N39 is also unusual among the feldspar-rich rocks, having low total REE, low La/Yb, but high concentrations of Rb, Ba and Sr, and a positive Eu anomaly (Eu/Eu* = 1·3; Table 2). In contrast, N43 (Fig. 3b) has significantly higher REE concentrations than other feldspar-poor xenoliths, which correlates with the presence of both monazite and zircon in this sample.

The highest La/Yb ratios are found in the amphibole-bearing granulites 435-1 and 37-40 (i.e. 23·8 and 24·1, respectively), whereas the two phlogopite-rich xenoliths (436-11 and 435-2E; Fig. 3d) have the lowest La/Yb ratios (4·14 and 5·16, respectively) (Table 2). In contrast, although orthopyroxenite sample 436-24b has similar LREE, Ba, Nb and P contents to 436-11, it has significantly lower heavy REE (HREE), Zr, Ti and Y abundances and a much higher La/Yb ratio (22·9). As will be shown in the next section, it is likely that the trace element composition of sample 436-24b has been contaminated by the host lamprophyre.

The two felsic granulites (N41-7, N57L) are leucosomes of migmatitic xenoliths. Their trace element compositions (Fig. 3c) resemble those of the feldspar-rich mafic granulites, except that N41-7 has a positive Eu anomaly (Eu/Eu* = 1·3). Concentrations of P, Sr, La, K and to a lesser extent Rb and Ba are the same in both the leucosome and mesosome of sample N57, but the leucosome (N57L) has significantly lower concentrations of all REE except La, giving it a higher La/Yb ratio than the mesosome (N57M), i.e. 15·5 vs 7·0. The REE pattern of the phlogopite-rich band (N57Ph) in this sample (not shown) is similar to that of the leucosome, but more LREE enriched (Table 2).

Figure 3f shows the trace element patterns for the composite xenolith 435-2, i.e. the phlogopite-rich 'eclogitic' granulite (435-2E) crosscut by a pyroxenite vein

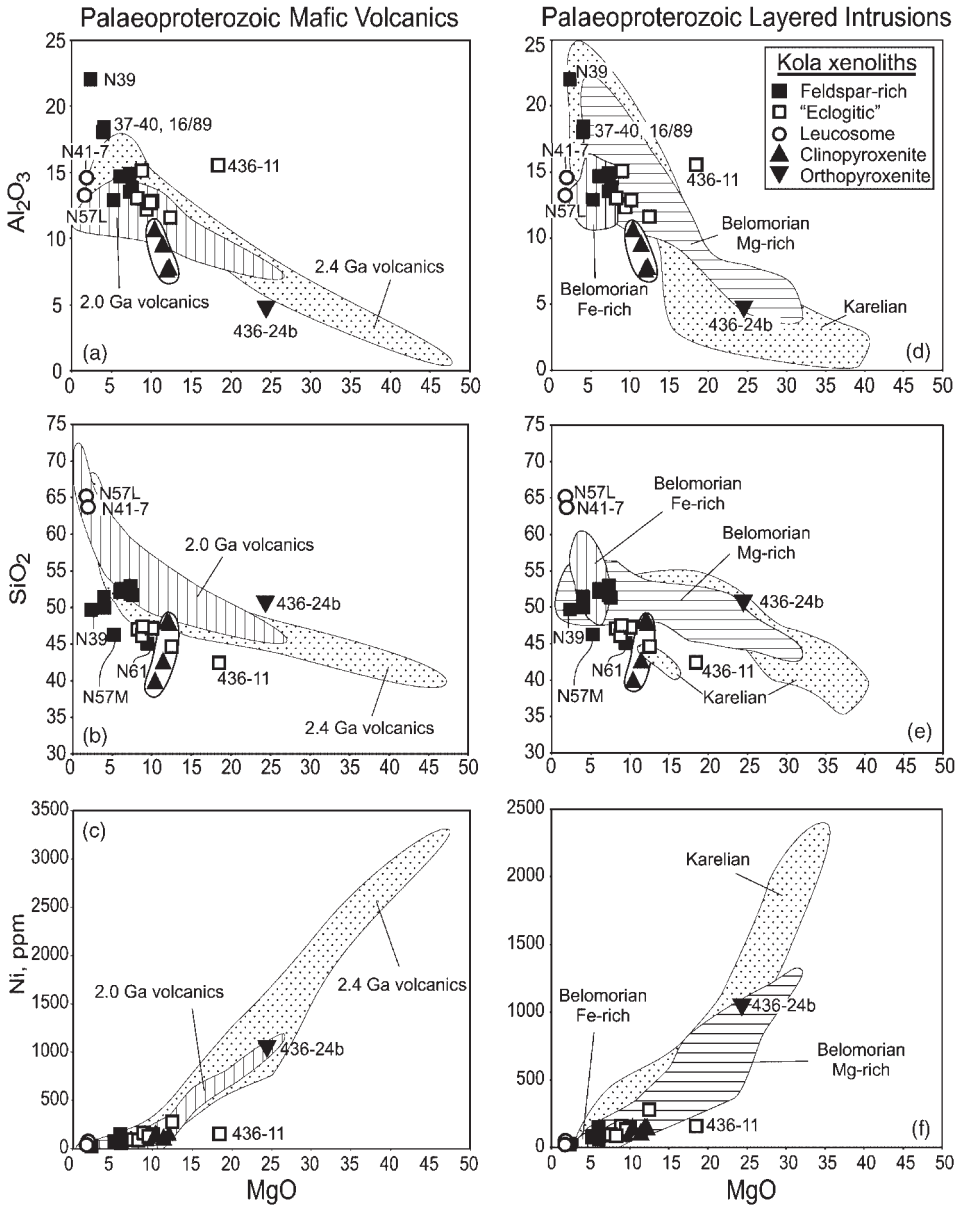

Fig. 2. Variation diagrams of MgO vs wt % Al_2O_3 (a and d), wt % SiO_2 (b and e) and ppm Ni (c and f) for Kola xenoliths, compared with Palaeoproterozoic rocks from the Belomorian Mobile Belt and Karelia. Data sources for Palaeoproterozoic layered intrusions include Sharkov *et al.* (1994, 1995, 1999), Snyder *et al.* (1995, 1996), Amelin & Semenov (1996), Higgins *et al.* (1996), Chistyakov *et al.* (1997) and Lobach-Zhuchenko *et al.* (1998). Data sources for Palaeoproterozoic extrusives include Amelin & Semenov (1996), Puchtel *et al.* (1996, 1997, 1998) and Sharkov *et al.* (1997).

(435-2P). The two patterns differ conspicuously. The eclogitic granulite has a fairly smooth pattern, whereas the associated pyroxenite has a very irregular pattern that is enriched in REE, but depleted in high field strength elements (HFSE). The lack of enrichment in the large ion lithophile elements (LILE) reflects the significantly lower modal abundances of amphibole and mica in the pyroxenite relative to the 'eclogitic' granulite host. The REE pattern for the pyroxenite is concave downward, similar to that of clinopyroxene crystallized from an LREE-enriched basaltic melt.

The coarse-grained vein pyroxenite of sample 435-2 is similar to the finer-grained amphibole-rich pyroxenites, 436-15a and 436-15b (Fig. 3e), in that all are LREE enriched and strongly depleted in P. However, 436-15a and 436-15b are enriched in Nb, which may indicate that they formed in equilibrium with an alkaline magma, or that the amphibole was derived from an alkaline melt.

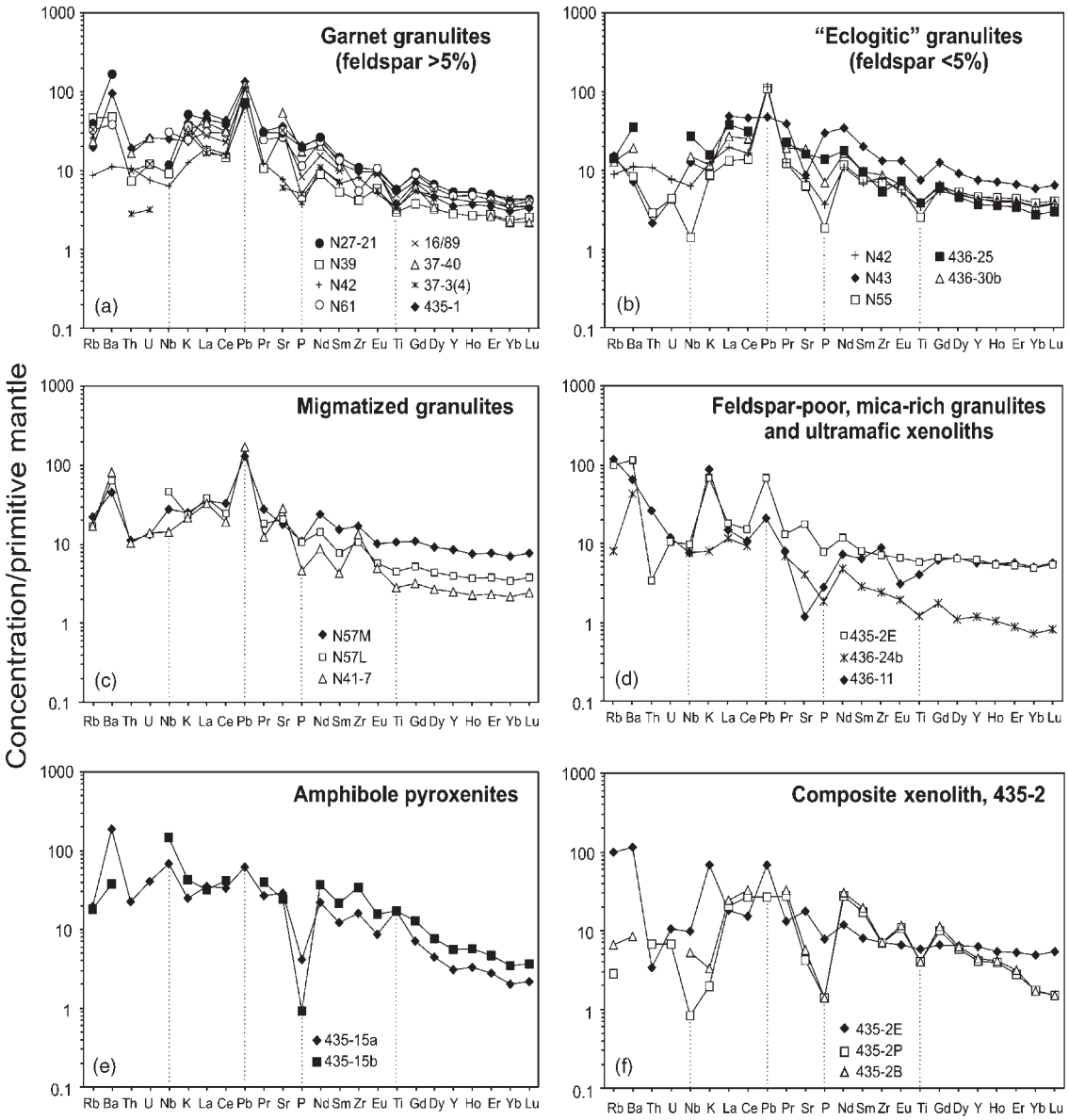

Fig. 3. Primitive-mantle-normalized incompatible trace element plots for various Kola xenolith groups. Feldspar-poor 'eclogitic' granulites have plagioclase contents $\leq 5\%$ (Kempton *et al.*, 1995). Normalizing values are from Sun & McDonough (1989). N42 has been plotted in both (a) and (b) to indicate the transitional nature of the patterns.

In contrast, coarse-grained pyroxenite 435-2 has much lower Rb, Ba, K, Nb and Sr contents (Fig. 3f), consistent with its lower modal abundance of amphibole.

Fig. 4 is a primitive-mantle-normalized diagram of the average composition of Kola granulite xenoliths compared with averaged values for Palaeoproterozoic layered intrusions, komatiites and picrites from the Baltic Shield. The Kola granulite xenoliths are similar in overall pattern shape to the Palaeoproterozoic rocks, but are significantly more enriched in incompatible trace elements than most of these (i.e. the Vetreney komatiites and Onega picrites and the Mg-series layered intrusions from the Belomorian Mobile Belt and Karelia). However, the Fe-rich layered intrusion series has a very similar pattern to the Kola granulite xenoliths, differing only in having slightly lower Nb, Sr, P and higher Ti. The Kola granulites are also similar to the Archaean lower-crustal composition of Rudnick & Fountain (1995), but again the Kola granulites have significantly higher concentrations of most elements, particularly the LREE, Nb, U and P.

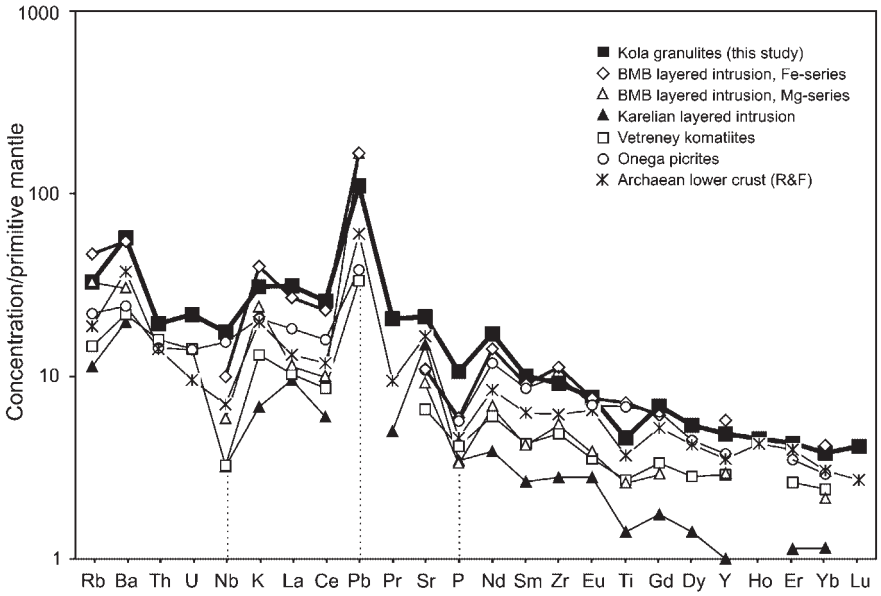

Fig. 4. Primitive-mantle-normalized incompatible trace element plots for average Kola granulites compared with average Archaean lower crust of Rudnick & Fountain (1995), and average compositions for various Palaeoproterozoic rocks. Data sources as in Fig. 2. Normalizing values are from Sun & McDonough (1989).

Nd isotope data

The Sm–Nd isotope data for the Kola xenoliths are listed in Table 3 and plotted in $^{143}Nd/^{144}Nd$ vs $^{147}Sm/^{144}Nd$ diagrams in Fig. 5. Although the scatter of the data points does not yield precise isochronous relationships, whole rock and constituent minerals (notably garnets) for samples 37-3(4), 37-40 and 16/89 form linear arrays that are in each case consistent with an age of ~1·5 Ga (Fig. 5a–c). Similarly, most of the whole-rock analyses for the granulites lie on or near the same array (Fig. 5d).

The amphibole pyroxenites, the ultramafic xenolith 436-24b and the phlogopite-rich band of migmatitic xenolith N57 lie off the granulite array and plot in a position intermediate between the array and the compositions of the host lamprophyres (Fig. 5d). In the case of 436-24b and N57Ph, this trend may indicate contamination by the host lamprophyre during transport to the surface. The coarse-grained vein pyroxenite, 435-2P, has an isotopic composition similar to the granulite xenoliths, although distinct from the metasomatized granulite with which it is in contact (Table 3). Excluding 436-24b, present-day ε_{Nd} values for whole-rock samples range from −6 to −27, but most lie within the range of −14 to −27 (Table 3). The highest values (least negative ε_{Nd}) are from phlogopite-rich sample 436-11 and the amphibole pyroxenites. Depleted mantle model ages (T_{DM}, t_1 = 1·5 Ga) have been calculated using the DePaolo *et al.* (1991) three-stage evolution scheme. These values range from 2·0 to 2·8 Ga, but most range from 2·4 to 2·6 Ga (Table 3).

Many of the xenoliths contain trace amounts of carbonate, analcime and/or chlorite that may have been introduced after exhumation from the lower crust. Therefore, to determine whether the isotope systematics of these samples were compromised by later fluid–rock interaction after exhumation, we performed a pilot study of two samples. Samples N39 and N41-7 were leached in hot 6M HCl for ~30 min. Obviously, this leaching procedure assumes that the primary minerals are not affected, which may not be valid because trace phases such as apatite and scapolite can be partially removed, as well as Na-rich plagioclase. In both cases, the leached samples have higher $^{143}Nd/^{144}Nd$ ratios than their unleached counterparts (Table 3), indicating that the material that has been removed had a low (crustal) $^{143}Nd/^{144}Nd$ ratio. Significant contamination by the host lamprophyres is thus unlikely for most samples, and the low values are probably the result of removal of minor amounts of plagioclase and/or primary trace phases such as apatite, which tend to have lower Nd isotope values (see Table 3).

Sr isotope data

The Rb–Sr isotope data are listed in Table 3 and plotted in an $^{87}Sr/^{86}Sr$ vs $^{87}Rb/^{86}Sr$ isochron diagram in Fig. 6. The present-day $^{87}Sr/^{86}Sr$ ratios of most of the garnet granulite xenoliths (Table 3) vary from 0·7052 to 0·7186, but this range of isotope ratios is clearly unsupported by the current $^{87}Rb/^{86}Sr$ of the rocks, suggesting that Rb

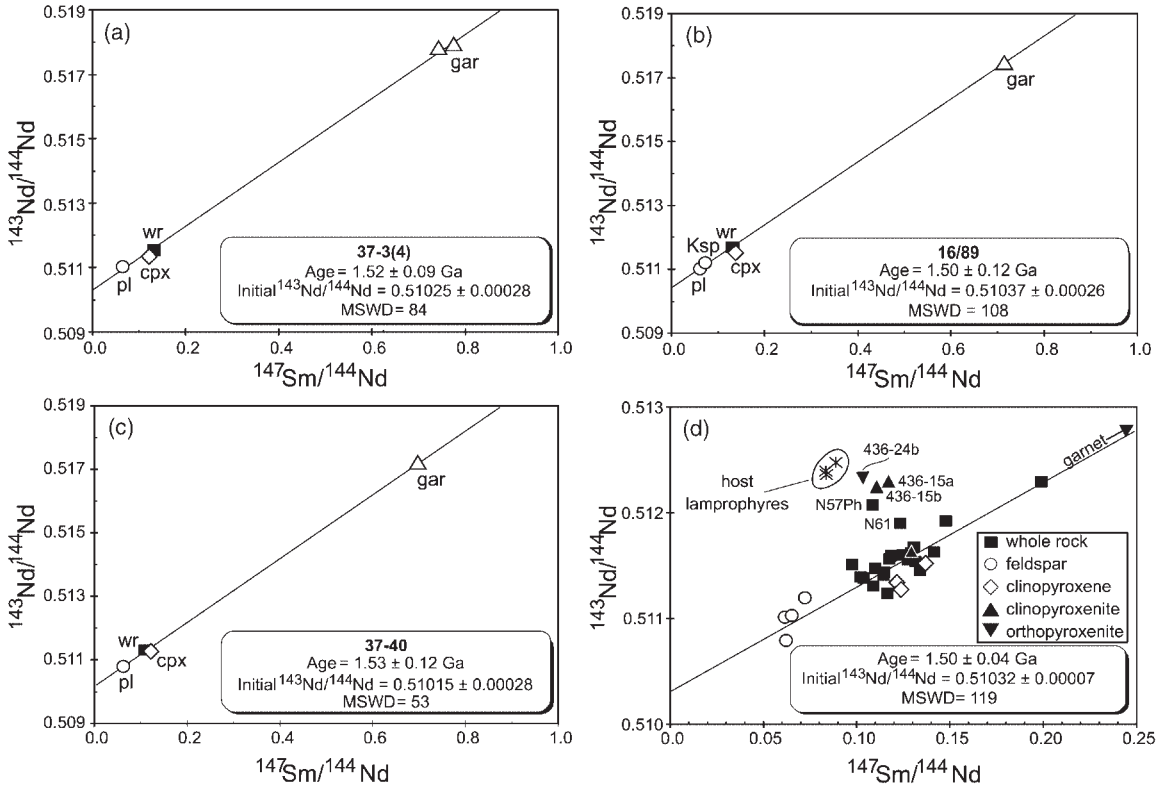

Fig. 5. $^{143}Nd/^{144}Nd$ vs $^{147}Sm/^{144}Nd$ isochron diagrams. Ages calculated using ISOPLOT/Ex (Ludwig, 1998).

has been lost from some samples. A much higher measured $^{87}Sr/^{86}Sr$ value (0·9564) is found in the phlogopite-rich sample 436-11; a regression of the data including this sample yields an 'errorchron' apparent age of ~1·9 Ga. This age may be indicative of the minimum age of phlogopite metasomatism in 436-11. In contrast to the Nd isotope results, there is no clear distinction between the pyroxenites, the granulites and the host lamprophyres in $^{87}Sr/^{86}Sr$, although the fine-grained amphibole pyroxenites tend to have lower $^{87}Sr/^{86}Sr$ than the coarse-grained pyroxenite 435-2P.

The effect of 6M HCl leaching on the isotopic composition of samples N39 and N41-7 is to reduce the measured $^{87}Sr/^{86}Sr$ ratios slightly (Table 3). The leachate from N39 has an $^{87}Sr/^{86}Sr$ of 0·7120. Because most of the analysed xenoliths have much lower $^{87}Sr/^{86}Sr$ values than this, if they have been affected by mild alteration, their true $^{87}Sr/^{86}Sr$ ratios may be slightly lower than the measured ones.

Pb isotope data

Geochronology

Pb isotope data are reported in Tables 4 and 5 and shown graphically in Fig. 7a–f. The isotopic ratios for the Kola xenoliths range widely in value from relatively unradiogenic ($^{206}Pb/^{204}Pb$ = 15·52, sample 37-40) to moderately radiogenic ($^{206}Pb/^{204}Pb$ = 22·47, sample 436-11). In a $^{207}Pb/^{204}Pb$ vs $^{206}Pb/^{204}Pb$ plot, the whole-rock data points for all samples scatter considerably about a best-fit line, which yields a poorly constrained isochron age of 2·23 ± 0·47 Ga [mean square weighted deviation (MSWD) = 128; Fig. 7a]. Because the xenolith suite may include some rocks with different petrogenetic histories, the observed scatter is perhaps not surprising. However, high-precision Pb isotope analyses have recently been determined at NIGL using the Tl-doping method available for PIMMS (plasma-ionization, multi-collector mass spectrometry) on a new suite of samples from the same localities; these new data indicate that at least some of the scatter is analytical in origin (A. J. W. Markwick & P. D. Kempton, unpublished data, 1999).

The effect of 6M HCl leaching on samples N39 and N41-7 is to preferentially remove the radiogenic isotopes and reduce the ratios in the leached fractions (Table 5). The significant differences in isotopic composition between leached and unleached fractions attest to the existence of an appreciable soluble component in both whole rocks, but no further attempt was made to identify it mineralogically. The isochron age calculated from the combination of sample N39 unleached whole rock,

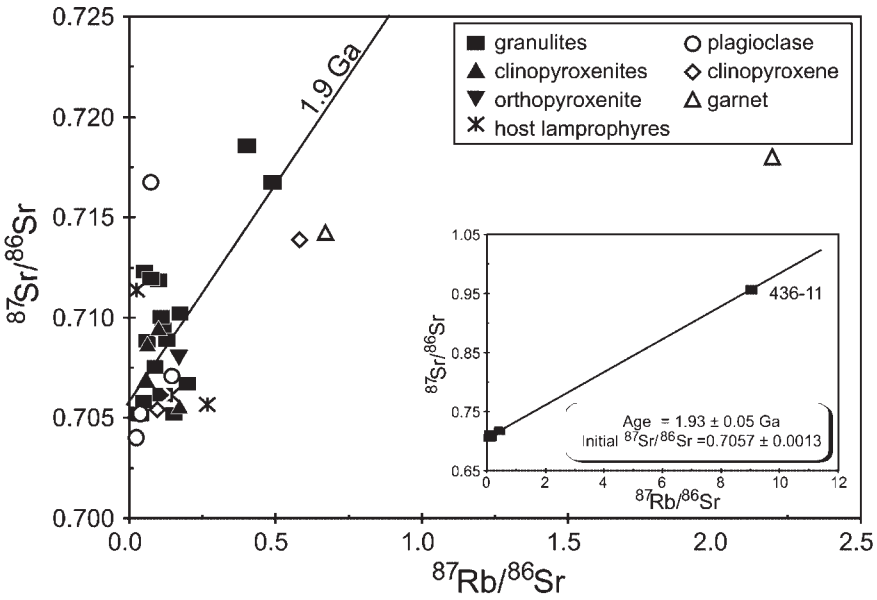

Fig. 6. $^{87}Sr/^{86}Sr$ vs $^{87}Rb/^{86}Sr$ isochron diagram. Age calculated using ISOPLOT/Ex (Ludwig, 1998).

leached whole rock and leachate is 2·12 ± 0·11 Ga (MSWD = 0·9; Fig. 7b); a similar but less precise age of 1·97 ± 0·46 Ga is calculated for the unleached and leached whole-rock pair of sample N41-7. These ages are similar to that calculated for all of the xenolith whole-rock samples, which suggests that a primary Pb-bearing phase is predominantly being removed. Hence, we feel confident in using the unleached whole-rock data to characterize the Pb isotope systematics of the xenoliths.

Assuming that isotopic equilibration or re-equilibration is more likely to have occurred on the scale of a single xenolith than throughout the entire suite, mineral separates from three of the xenoliths [samples 37-40, 37-3(4) and 16/89] were analysed to see whether they provided more precise internal isochrons. To reduce any complicating effects caused by introduction of an exotic labile Pb component subsequent to crystallization, the minerals were generally subjected to acid leaching before analysis. Leachates from feldspar and clinopyroxene have consistently more radiogenic compositions than the corresponding residues, whereas garnet leachates are less radiogenic, suggesting late Pb transfer among the minerals. Introduction of an exotic Pb from the host lamprophyre or during surface alteration might also be entertained, but although the leachates encompass a wide range in isotopic composition, they show no tendency to trend toward that of the lamprophyre. The leachate isotopic compositions have been omitted from the calculated isochron ages, for which only whole-rock, plagioclase, garnet and clinopyroxene analyses are included.

The minerals from each of the three xenoliths form reasonable linear arrays on $^{207}Pb/^{204}Pb$ vs $^{206}Pb/^{204}Pb$ (and $^{208}Pb/^{204}Pb$ vs $^{206}Pb/^{204}Pb$) plots, but with distinctly different slopes and, consequently, different ages. On the basis of their uncertainties and MSWD, these arrays may be regarded as producing borderline isochron ages. From oldest to youngest, they are calculated as 2·56 ± 0·41 Ga for sample 37-40 (Fig. 7c), 1·86 ± 0·51 Ga for sample 16/89 (Fig. 7d), and 1·23 ± 0·40 Ga for sample 37-3(4) (Fig. 7e). Furthermore, the two older isochron ages agree moderately well with those derived from the intersection of the arrays with the Stacey & Kramers (1975) growth curve in the respective $^{207}Pb/^{204}Pb$ vs $^{206}Pb/^{204}Pb$ (Fig. 7c–e) and $^{208}Pb/^{204}Pb$ vs $^{206}Pb/^{204}Pb$ (not shown) plots. These $^{207}Pb/^{204}Pb$ vs $^{206}Pb/^{204}Pb$ and $^{208}Pb/^{204}Pb$ vs $^{206}Pb/^{204}Pb$ intercept ages are, respectively, 2·66 and 2·75 Ga for sample 37-40, and 2·04 and 2·25 Ga for sample 16/89, and would seem to confirm a rather straightforward two-stage interpretation of these isochrons. The youngest isochron age obtained for sample 37-3(4) must record a more complex history, however, as evidenced by the large disparity between its $^{207}Pb/^{204}Pb$ vs $^{206}Pb/^{204}Pb$ and $^{208}Pb/^{204}Pb$ vs $^{206}Pb/^{204}Pb$ intercept ages of 0·99 and 2·00 Ga, respectively, and by the positioning of the two plagioclase data points far to the left of the growth curve. Such displacement of the initial Pb isotopic composition generally signifies earlier residence in an elevated U/Pb environment followed by later residence in a reduced U/Pb environment, and may indicate that some significantly older Archaean protolith contributed to the formation of this particular xenolith. None the less, it is doubtful that initial isotopic heterogeneity should exist among the mineral phases of a single xenolith, and the meaning of the 1·23 ± 0·40

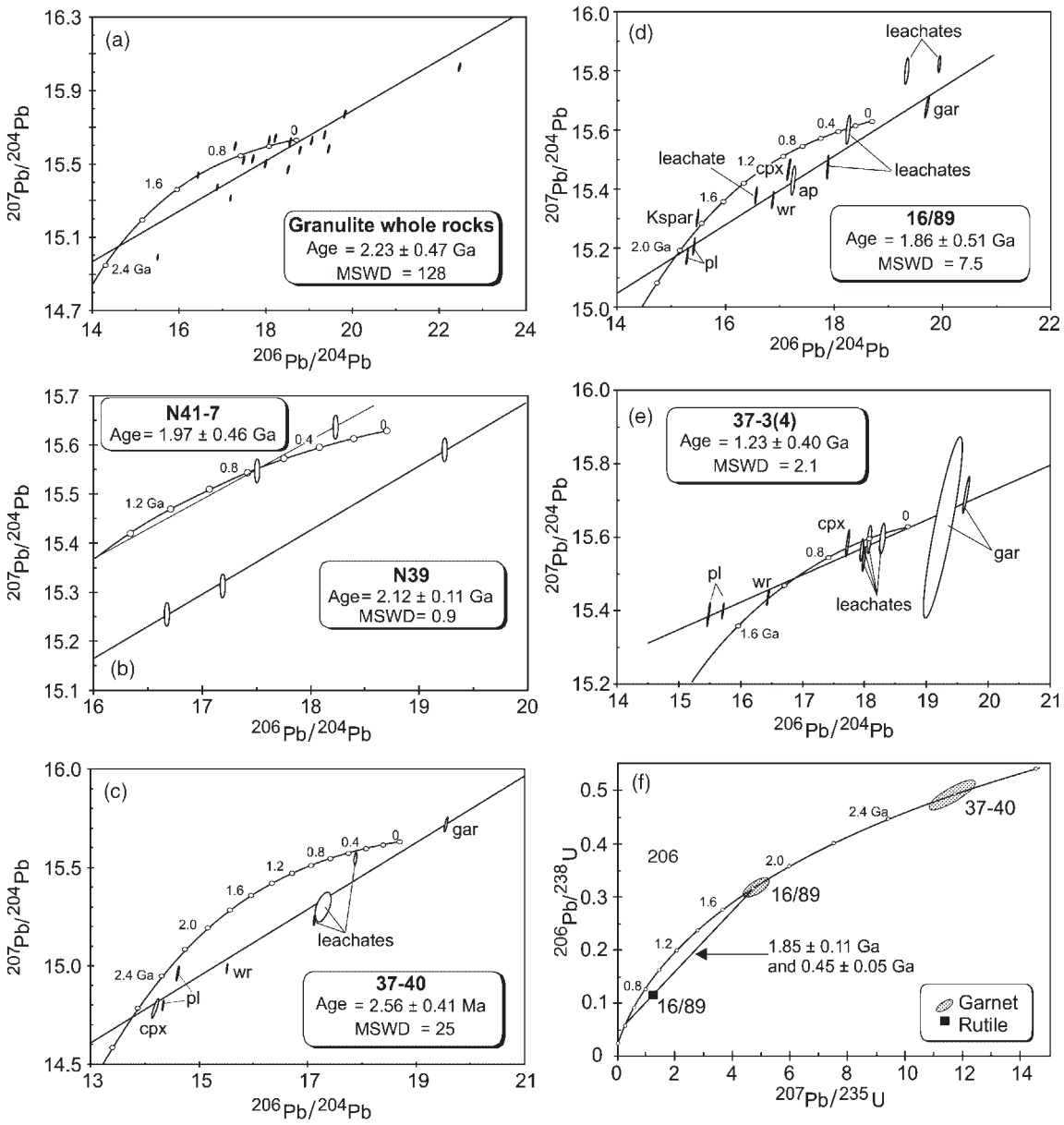

Fig. 7. (a–e) Plots of $^{207}Pb/^{204}Pb$ vs $^{206}Pb/^{204}Pb$ for Kola granulite xenolith whole-rock and mineral samples. Ages calculated using ISOPLOT/Ex (Ludwig, 1998). Mineral isochron regressions include whole-rock, clinopyroxene, garnet and plagioclase fractions only. The analysis of Gar (1) has been omitted from the regression of sample 37-3(4) (see Table 4) because of its high analytical error. (f) U–Pb concordia plot of garnet and rutile fractions from samples 37-40 and 16/89.

Ga internal isochron for sample 37-3(4) is unclear. The age is not supported by any other isotopic data, and the geological record shows this to be a time of crustal stability rather than orogenic or magmatic activity.

Additional evidence for the validity of the crystallization ages of the two older individual xenoliths is provided by a U/Pb concordia plot of the garnets from samples 37-40 and 16/89 (Fig. 7f). The radiogenic Pb contents were calculated by making initial Pb corrections using the least radiogenic isotopic composition observed in coexisting plagioclase. The garnets from the two samples give concordant ages of 2·59 and 1·85 Ga, respectively, consistent within error limits with the isochron ages and strongly supportive of closed-system behaviour. A rutile from sample 16/89, on the other hand, plots significantly off concordia and can be interpreted as lying on a discordia line between 1·83 and ~0·4 Ga. If the rutile is a primary phase of the xenolith, this discordance reflects severe disturbance of the mineral's isotopic system, presumably at the time of incorporation of the xenolith into the host

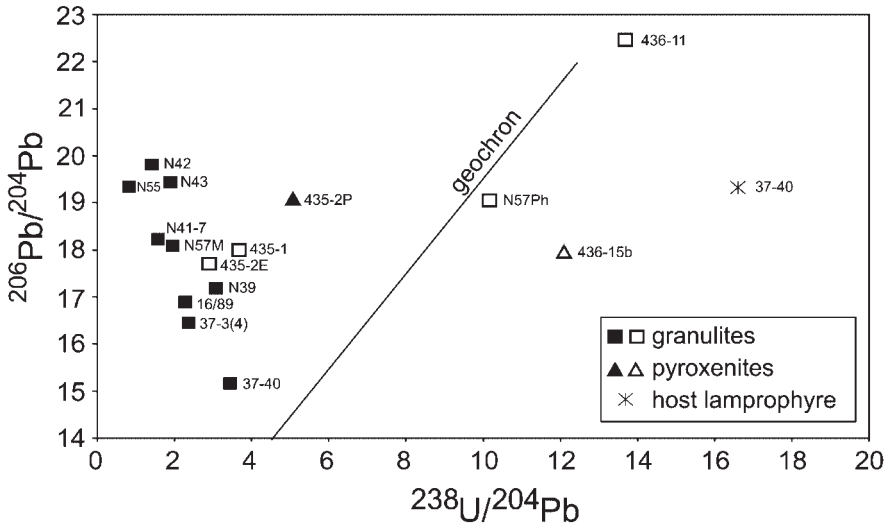

Fig. 8. $^{238}U/^{204}Pb$ vs $^{206}Pb/^{204}Pb$ plot of Kola whole-rock and mineral samples. Shown for reference is a 4·6 Ga geochron drawn through an initial Canyon Diablo $^{206}Pb/^{204}Pb$ = 9·31 and $^{238}U/^{204}Pb$ (μ) = 0. Open symbols for granulites and pyroxenites indicate samples for which hydrous phases form >5% of the mode.

lamprophyre. U–Pb data for garnet from sample 37-3(4) (not shown in Fig. 7f) display strongly reversed discordance, indicating either open-system behaviour for the garnet or appreciably different closure conditions for plagioclase and garnet. It is also possible that this xenolith retains an isotopic heterogeneity among its mineral phases inherited at the time of crystallization, which could prevent determination of a meaningful age.

$^{238}U/^{204}Pb$ vs $^{206}Pb/^{204}Pb$

Figure 8, a $^{238}U/^{204}Pb$ vs $^{206}Pb/^{204}Pb$ plot of the whole rocks, clearly shows that the U/Pb ratios observed in most of the Kola xenoliths have been substantially reduced from the time-integrated values required by their Pb isotopic composition. That is, with the exception of granulite 436-11 and pyroxenite 436-15b, the xenoliths plot well to the left of the geochron, with $^{238}U/^{204}Pb$ values ranging from 0·82 to 5·08 (or, for the granulites only, 3·68). Perhaps the most striking feature of the plot is that the granulites, with the exception of the phlogopite-rich sample 436-11, form an array with a distinctly negative slope, indicating an inverse relationship between U/Pb and $^{206}Pb/^{204}Pb$. A similar negative slope is seen in a $^{235}U/^{204}Pb$ vs $^{207}Pb/^{204}Pb$ plot, but in a $^{232}Th/^{204}Pb$ vs $^{208}Pb/^{204}Pb$ plot the trend is essentially vertical. In comparison with the granulites, the one analysed host lamprophyre, sample 37-42, has a $^{238}U/^{204}Pb$ of 16·6 and plots well to the right of the geochron.

The radiogenic end of the granulite array consists of the plagioclase-poor, 'restitic' rocks, whereas the more feldspar-rich rocks occupy the lower $^{206}Pb/^{204}Pb$ and higher U/Pb end of the array. If the present-day U/Pb ratios of the granulite xenoliths represent their closed-system values since crystallization, there is no way to account for the heterogeneity in isotopic composition by *in situ* radioactive decay. In fact, the spread in isotopic composition would increase backward in time because of the higher U/Pb in the least radiogenic rocks. On the other hand, giving age credence to the isochron in Fig. 7a requires that a substantial proportion of the spread in isotopic composition was produced by radioactive decay since crystallization of the xenoliths. In such a case the correlation between lithology and U/Pb is better explained by relatively recent, mineralogically controlled, U loss than as an attribute of the rock's original composition. Disturbance of the U/Pb in the granulites, however, can bring into question the validity of the whole-rock isochron age because any change in this ratio violates the basic dating assumption of a closed system. If, for example, as will be speculated, considerable U loss occurred at the time of Devonian lamprophyre emplacement, the calculated granulite isochron age of 2·23 $\pm$ 0·47 Ga could be as much as 200 my too old.

Comparisons with Palaeoproterozoic surface rocks of the Baltic Shield and lower-crustal xenoliths worldwide

The Pb isotope data for the Kola xenoliths together with local Palaeoproterozoic surface rocks are shown in $^{207}Pb/^{204}Pb$ vs $^{206}Pb/^{204}Pb$ and $^{208}Pb/^{204}Pb$ vs $^{206}Pb/^{204}Pb$ plots in Fig. 9a and b, respectively. In the $^{207}Pb/^{204}Pb$ vs $^{206}Pb/^{204}Pb$ plot, the majority of the xenoliths overlap the 2·0 Ga Onega plateau basalts and picrites and the 2·0 Ga meta-igneous granulites of the Lapland granulite belt. A few of them, predominantly the migmatitic rocks (e.g.

samples N41-7 and N57), have slightly higher $^{207}Pb/^{204}Pb$ for a given $^{206}Pb/^{204}Pb$ and extend into the fields of the Lapland meta-sediments and the 2·4 Ga Karelian layered intrusions. In addition, the plagioclases from samples 37-40, 16/89 and 37-3(4) form a trend in the $^{207}Pb/^{204}Pb$ vs $^{206}Pb/^{204}Pb$ plot (Fig. 9a), which overlaps the trend observed for plagioclases from the layered intrusions of the Olanga complex (Amelin & Neymark, 1998). The similarity in isotopic composition of the Kola xenoliths to presumed contemporaneous mafic igneous rocks of the Belomorian mobile belt and Lapland–Umba granulite belt is highly supportive evidence of a common origin. This argument is further strengthened when one recognizes the unique composition of these xenoliths relative to other lower-crustal xenoliths worldwide (Fig. 9c). About half of the Kola samples lie to the right of the geochron, and in this way resemble Phanerozoic xenolith suites more than other Proterozoic ones.

In contrast to the overlap in compositions in $^{207}Pb/^{204}Pb$ vs $^{206}Pb/^{204}Pb$ (Fig. 9a), the Kola granulites are unlike most other rocks from the Baltic region (Fig. 9b) or other lower-crustal granulites worldwide (Fig. 9d) in $^{208}Pb/^{204}Pb$ vs $^{206}Pb/^{204}Pb$. Several of the samples have unusually radiogenic $^{208}Pb/^{204}Pb$ (>42), including not only the phlogopite-rich sample 436-11 but also four anhydrous garnet granulites (samples N42, N43, N55 and N61) and the coarse-grained vein pyroxenite 435-2P. One 'eclogitic' granulite (436-30b) and the orthopyroxenite (436-24b), as well as the amphibole pyroxenites (436-15a and 436-15b), lie distinctly below the array defined by most of the Kola xenoliths in the $^{208}Pb/^{204}Pb$ vs $^{206}Pb/^{204}Pb$ plot. None of the xenoliths consistently overlap or trend toward the isotopic composition of the host lamprophyre, implying that they have been minimally contaminated by it. It should be noted that no attempt has been made to age correct the Pb composition of the xenoliths because we do not know when the isotope ratios and measured U/Pb were decoupled.

$^{40}Ar/^{39}Ar$ data

$^{40}Ar/^{39}Ar$ high spatial resolution UV laser analyses of four phlogopite grains from metasomatized xenolith sample 436-11 yield young ages as low as 410 ± 164 and 412 ± 90 Ma at the rims, rising steadily to a maximum age of 2·23 ± 0·02 Ga in one grain centre (Fig. 10 and Table 6). An unweighted mean age of 2·10 ± 1·0 Ga was calculated from the five oldest line traverse ages obtained from the largest and best preserved phlogopite grain in this sample. The 410 Ma rim ages correspond very closely to the Devonian eruption age of the diatreme (Fig. 10), whereas the mean 2·10 ± 0·1 Ga core age is consistent with the Nd model age range of 2·0–2·8 Ga, a minimum $^{87}Sr/^{86}Sr$ vs $^{87}Rb/^{86}Sr$ metasomatic age of 1·9 Ga from the same xenolith, and $^{207}Pb/^{204}Pb$ vs $^{206}Pb/^{204}Pb$ whole-rock ages of 2·23 ± 0·47 Ga for the xenolith suite.

The conundrum of old ages preserved in phlogopites found in metasomatized xenoliths and phenocrysts in kimberlite magmas has been interpreted as excess ^{40}Ar introduction (Phillips & Onstott, 1986, 1988; Phillips, 1990), thereby deeming the Ar–Ar ages geologically meaningless. Excess ^{40}Ar, defined as ^{40}Ar that is not produced during *in situ* K decay, is believed to be introduced as a result of the presence of elevated fluid pressures at depth during phlogopite formation. However, studies by Pearson *et al.* (1997) have cast doubt on this interpretation, suggesting that old 2·1–2·4 Ga $^{40}Ar/^{39}Ar$ ages from xenolithic phlogopites analysed from the Udachnaya kimberlite in Siberia are geologically significant. In these instances, the phlogopite grains may retain Ar signatures reflecting the antiquity of either the lithosphere, or the source regions from which the fluids originated. However, at depth the temperature would be above the Ar blocking temperature for phlogopite (~400–450°C) and any ages preserved will not reflect simple Ar blocking temperature ages.

From the $^{40}Ar/^{39}Ar$ UV laser data from sample 436-11, we suggest that the old 2·10 ± 0·1 Ga ages preserved in the grain cores are phlogopite formation ages and hence determine the age of metasomatism, suggesting that the Ar budget in the lower crust under the northern Baltic Shield has remained undisturbed since ~2·1 Ga. The lack of orogenic processes in the northern Baltic Shield is confirmed by the presence of flat-lying 0·9–1·4 Ga Riphean sediments (Mitrofanov, 1995). Ages remained undisturbed until the onset of the eruption of the lamprophyre diatreme and the second metasomatic event resulting in the crystallization of hornblende at ~394 Ma (Beard *et al.*, 1996). The incorporation of the xenolith into the ascending lamprophyre magma resulted in degassing and ^{40}Ar loss from the grain boundaries of the phlogopite grains (Fig. 10). Assuming volume diffusion

Fig. 9. (*opposite*) $^{207}Pb/^{204}Pb$ vs $^{206}Pb/^{204}Pb$ and $^{208}Pb/^{204}Pb$ vs $^{206}Pb/^{204}Pb$ plots comparing Pb isotopes in Kola granulite and pyroxenite xenoliths with some surface Palaeoproterozoic rocks of the region (a and b, respectively), and other lower-crustal xenoliths worldwide (c and d, respectively). Data sources as follows: Lapland granulites, Bernard-Griffiths *et al.* (1984); Onega plateau volcanics, Puchtel *et al.* (1998); Karelian layered intrusions and plagioclase, Amelin & Neymark (1998). The sample outliers in (c) and (d) include a felsic granulite xenolith from the Geronimo Volcanic Field (GVF, Kempton *et al.*, 1990) and meta-igneous(?) granulite xenoliths from the Snake River Plain (SRP; Leeman *et al.*, 1985). Symbols used for Kola xenoliths are the same in all figures. Symbols used for Lapland granulites in (b) are as identified in (a).

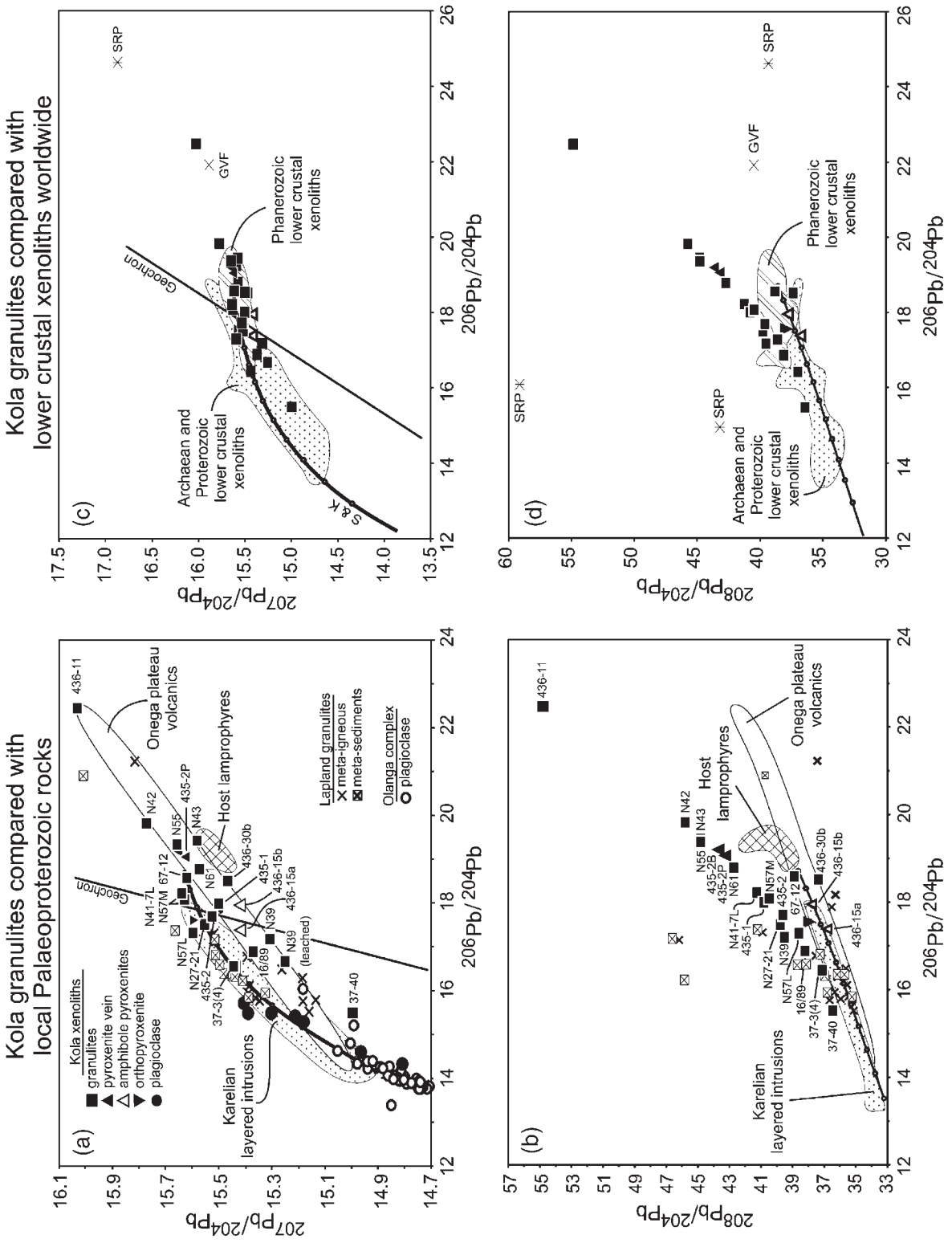
Kola granulites compared with local Palaeoproterozoic rocks
Kola granulites compared with lower crustal xenoliths worldwide
(a)
(b)
(c)
(d)
Kola xenoliths
granulites
pyroxenite vein
amphibole pyroxenites
orthopyroxenite
plagioclase
Geochron
Onega plateau volcanics
Host lamprophyres
Karelian layered intrusions
Lapland granulites
meta-igneous
meta-sediments
Olanga complex
plagioclase
436-11
N42
N55
435-2P
N43
N61
67-12
N41-7L
N57M
N27-21
435-2
37-3(4)
N57L
16/89
N39
436-30b
435-1
436-15b
436-15a
N39 (leached)
37-40
Archaean and Proterozoic lower crustal xenoliths
Phanerozoic lower crustal xenoliths
GVF
SRP
S&K
206Pb/204Pb
207Pb/204Pb
208Pb/204Pb

Fig. 9.

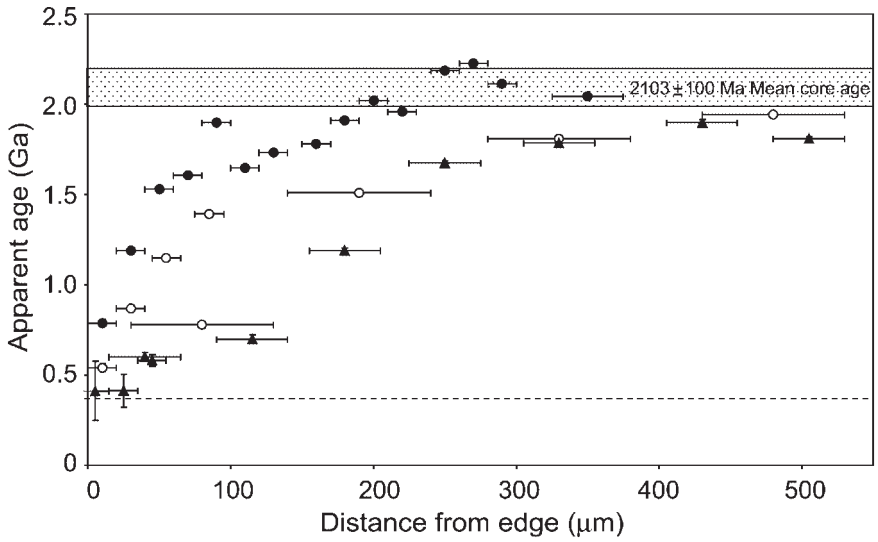

Fig. 10. $^{40}Ar/^{39}Ar$ age vs distance from rim graphs for UV laser traverses across phlogopite grains from xenolith 436-11 indicating ^{40}Ar diffusive loss. ●, ○, phlogopite grain 1 (traverses 1 and 2, respectively); ▲, phlogopite grain 2 (traverse 1).

behaviour of Ar in the phlogopites and with an approximate estimate of the diatreme magma temperature, ^{40}Ar loss profiles can be used to access the length of time the xenolith spent outgassing in the lamprophyre magma and by inference can yield approximate diatreme ascent times. Assuming magma temperatures of 1100 and 1200°C, three radiogenic ^{40}Ar diffusion profiles yielded ascent rates of between 2·1–9·3 days and 0·5–2·2 days, respectively.

DISCUSSION

Nature of the xenolith protoliths

Kempton *et al.* (1995) showed from major element arguments that most of the Kola mafic granulite xenoliths (i.e. plagioclase-rich garnet granulites) represent solidifed melts rather than igneous cumulates or meta-sediments. The similarity in LREE-enriched trace element patterns for the xenoliths supports this interpretation (Table 2, Fig. 3). The rocks tend to be hypersthene normative, suggesting a sub-alkaline precursor, so the most probable magmatic affinity for the protoliths is that of a tholeiitic basalt. However, primitive-mantle-normalized incompatible trace element plots (Fig. 3) do not resemble LREE-depleted N-MORB; instead, they are more akin to LREE-enriched continental flood basalt magmas. In fact, the Kola xenoliths share many of the major and trace element characteristics of the Palaeoproterozoic mafic rocks of the Kola Peninsula (Figs 2 and 4), believed to be part of one of the Earth's earliest large igneous provinces (Heaman, 1997; Sharkov *et al.*, 1999).

Garnet-rich, plagioclase-poor 'eclogitic' granulites (e.g. N43 and N55) have lower SiO_2 at a given MgO than Palaeoproterozoic volcanic rocks of the region (Fig. 2b and e), but this is consistent with the partial melting (migmatization) hypothesis proposed by Kempton *et al.* (1995), i.e. these particular samples are not representative of solidified melts, but restites.

Although very few pyroxenites have been analysed in this study, it is clear that there are two types in the xenolith suite. Their origins may be significantly different, although both types are LREE enriched (Fig. 3). One pyroxenite type is represented by a coarse-grained vein (435-2P) that crosscuts a mica-bearing 'eclogitic' granulite (435-2E). The second pyroxenite type is more fine grained and shows substantial replacement of primary pyroxene by secondary amphibole (40–50%). Although amphibole is rare in the granulite xenoliths, phlogopite may be present and is abundant (up to 45%) in some cases, which led Kempton *et al.* (1995) to propose that the Kola lower crust has been subjected to one or more metasomatic events.

In subsequent sections we attempt to constrain the timing of these various petrogenetic processes and place the Kola granulite xenoliths in the context of the known geological history of the region.

Age constraints and relationship with known upper-crustal events

Although the data presented in Figs 5–7 do not precisely date the Kola xenoliths, it has still been possible to place them, and the various stages of their evolution, within the context of the currently known geological history of the northern Baltic Shield. Petrographic, geochemical and mineralogical observations provide evidence for the

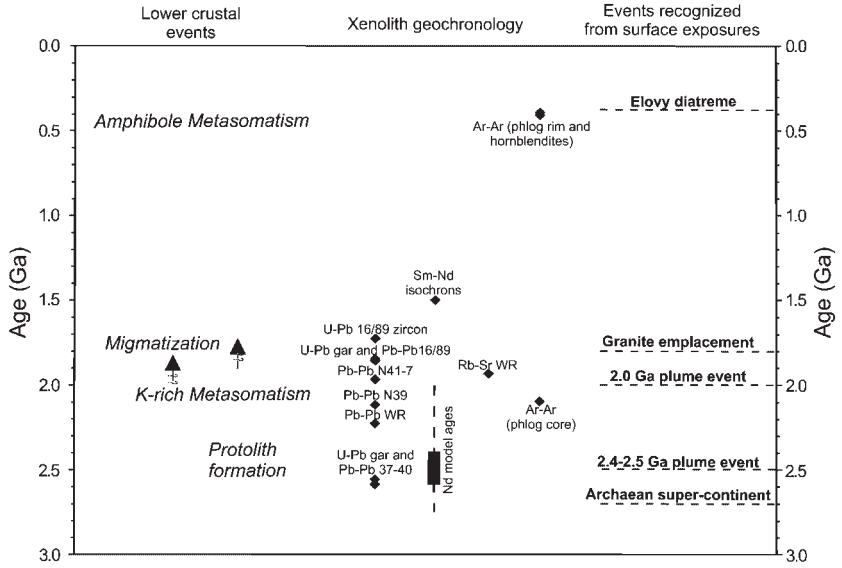

Fig. 11. Summary of the Kola xenolith geochronology and inferred lower-crustal events compared with magmatic and orogenic events identified from surface exposures.

occurrence of both metasomatism and partial melting (migmatization) subsequent to crystallization and metamorphism of the protoliths to granulite facies (Kempton *et al.*, 1995). Figure 11 summarizes our interpretation of the timing of these events from the available Rb–Sr, Sm–Nd, U–Pb and $^{40}Ar/^{39}Ar$ isotopic data, and these are described in more detail below.

Age of the protoliths and timing of metamorphism

The $^{143}Nd/^{144}Nd$ vs $^{147}Sm/^{144}Nd$ isochron diagrams (Fig. 5) suggest a minimum age for the granulites of 1·5 Ga. To our knowledge, this 'age' does not correspond to any known upper-crustal event. However, the Sm–Nd isochrons are mainly controlled by the compositions of the garnets, and therefore correspond to the time at which the granulites cooled through the blocking temperature for the Sm–Nd system in this mineral. This interpretation is consistent with the precise U–Pb age of 1·73 ± 0·02 Ga for zircon separated from sample 16/89 (Vetrin & Nemchin, 1998). Notably, all two-point Pl–Cpx Sm–Nd isochrons give 'ages' in the range of 0·84–1·2 Ga. This may be caused by later closure of Sm–Nd in plagioclase or its disturbance during interaction with the host magma.

Nd model ages (T_{DM}) calculated using the multi-stage Nd evolution scheme proposed by DePaolo *et al.* (1991) range from 2·0 to 2·8 Ga, but most range from 2·4 to 2·6 Ga (Table 3). This model assumes that the present-day measured isotopic values can be projected back to some time t_1, when the Sm/Nd either increased or decreased. Before time t_1, it is assumed that the granulites followed similar crustal evolution paths, approximated by an average crustal value; this value is used to project back to the depleted mantle evolution curve to derive T_{DM}. We have chosen 1·5 Ga as time t_1, i.e. the 'age' derived from $^{143}Nd/^{144}Nd$ vs $^{147}Sm/^{144}Nd$. If time t_1 is 1·7 Ga (the U–Pb zircon age) the difference to the calculated model ages is small. Even if a value of 2·0 Ga is assumed for t_1, the T_{DM} values average <4% higher than those calculated for a t_1 of 1·5 Ga. However, the best clustering of ages occurs when the T_{DM} values are calculated for $t_1 = 1{\cdot}5$ Ga.

The Nd model age calculations are summarized according to granulite type in Fig. 12. T_{DM} ($t_1 = 1{\cdot}5$ Ga) ages for most feldspar-rich garnet granulites, 'eclogitic' granulites and migmatitic leucosomes cluster at 2·4–2·6 Ga. One 'eclogitic' granulite (N43) and one garnet granulite (N42) have slightly older model ages of 2·75 and 2·70 Ga, respectively, whereas the metasomatized xenoliths extend to slightly younger ages of 2·0 Ga. The latter is not particularly surprising and is consistent with introduction of a more radiogenic Nd component during metasomatism. Similarly, contamination by the host lamprophyres is clearly responsible for the young model age (0·8 Ga) of orthopyroxenite 436-24b (see Table 3). However, the explanation for the spread to older model ages is less clear. One possibility is that this is due to mixing between younger Proterozoic (1·7 Ga) magmas and older Archaean crust. Alternatively, it may be a consequence of migmatization. Of the five xenoliths with Nd model ages between 2·6 and 2·8 Ga, two are 'eclogitic' (samples N55 and N43) and two are garnet granulites that are relatively plagioclase poor [samples 37-3(4) and N42]. The xenolith suite provides abundant evidence for

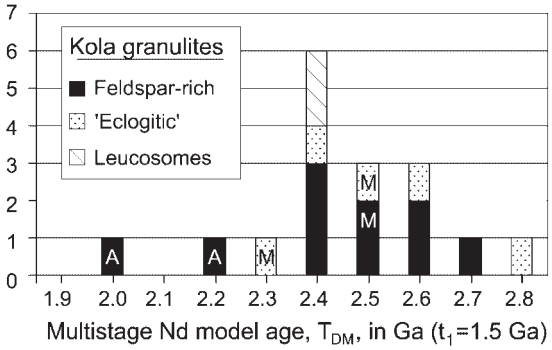

Fig. 12. Histogram summarizing Nd model ages for multi-stage method evolution. Orthopyroxenite sample 436-24b plots outside the diagram to the left with a model age of 0·85 Ga. Metasomatized samples containing significant modal abundances of amphibole or mica are indicated by the letters A and M, respectively.

migmatization, with leucosomes consisting predominantly of quartz and feldspar associated with melanosomes dominated by garnet and/or cpx ± feldspar and quartz (Table 1). This process would increase the Sm/Nd ratios of the residues and reduce the ratios in the melt portions. The result would be that the Nd model ages for the leucosomes would be lower, whereas those for the restites would be higher. Thus, lower Nd model ages would be expected in the more siliceous granulites (e.g. N41-7 and N57L) than in the plagioclase-poor, garnet-rich ('eclogitic' or 'restitic') samples such as N42, N43, N55 and N57M. Finally, a formation age some time between 2·4 and 2·6 Ga is consistent with the 2·23 ± 0·47 Ga ^{207}Pb–^{206}Pb isochron age of the granulite whole rocks (Fig. 7a), the 2·12 ± 0·11 Ga ^{207}Pb–^{206}Pb isochron age of N39 (Fig. 7b), the 2·56 ± 0·41 Ga ^{207}Pb–^{206}Pb isochron age of sample 37-40 (Fig. 7c) and the 2·59 Ga U–Pb age for garnet in sample 37-40 (Fig. 7f). When taken in conjunction with the similarities in chemical composition between the granulite xenoliths and exposed Palaeoproterozoic rocks of the region (Figs 2 and 4), these data strongly suggest that the granulite protoliths originated from the same magmatic event that gave rise to the widespread layered intrusions common throughout the northern Baltic Shield at 2·4–2·5 Ga.

A potential problem with this hypothesis is that the parental magmas of the Palaeoproterozoic mafic layered intrusions have ε_{Nd} (2·4 Ga) ranging from slightly positive to mostly negative values of −1 to −3 (Anderson & Sundvoll, 1995; Amelin & Semenov, 1996), which Snyder *et al.* (1996) have interpreted as evidence that the rocks were derived from enriched mantle source(s). In contrast, most Kola granulite xenoliths have positive ε_{Nd} when calculated for 2·4 Ga (Table 3). However, Lobach-Zhuchenko *et al.* (1998) showed that mixing of a mantle-derived picrite with local tonalites can explain the compositional variations of the layered intrusions from the Belomorian Mobile Belt, including their Nd isotope characteristics. They further argued that such a process also affected the komatiitic basalts of the Vetreny Belt and the layered mafic intrusions in the Karelian province, which have similar geochemical characteristics to the intrusions in the Belomorian Mobile Belt (Amelin *et al.*, 1995; Amelin & Semenov, 1996; Puchtel *et al.*, 1996, 1997). Thus, the differences between the ε_{Nd}(2·4 Ga) values of the exposed Palaeoproterozoic extrusive and plutonic rocks and the entrained lower-crustal xenoliths can be explained if the effects of crustal contamination are significantly less in the lower crust than at shallower levels. This is a reasonable suggestion if one considers that the lower crust is probably composed of underplated, mantle-derived, mafic igneous rocks, whereas the mid- and upper crust would almost certainly include a large component of metasediments.

Timing of migmatization

Accepting that the protoliths of the granulite xenoliths were formed between 2·4 and 2·6 Ga, the younger ages derived from $^{87}Sr/^{86}Sr$ vs $^{87}Rb/^{86}Sr$, $^{143}Nd/^{144}Nd$ vs $^{147}Sm/^{144}Nd$ and $^{207}Pb/^{204}Pb$ vs $^{206}Pb/^{204}Pb$ must reflect disturbances and/or resetting in response to subsequent events in the lower crust. For example, the 1·97 ± 0·46 Ga ^{207}Pb–^{206}Pb isochron based on migmatitic granulite N41-7 (Fig. 7b) may be indicative of such an event. Similarly, the 1·73 ± 0·02 Ga U–Pb zircon age of feldspar-rich granulite 16/89 (Vetrin & Nemchin, 1998) may indicate zircon growth in response to the thermal event that gave rise to migmatization. The same sample also gave a mineral ^{207}Pb–^{206}Pb isochron age of 1·86 ± 0·51 Ga (Fig. 7d) and a concordant U–Pb age of 1·83 Ga for a garnet separate (Fig. 7f), providing additional evidence of isotopic resetting at this time. Partial melting in the lower crust beneath the northern Baltic Shield at this time is consistent with the intrusion of granites and micaceous pegmatites at 1·8 Ga in the Belomorian Mobile Belt (Patchett & Kouvo, 1986; Glebovitsky, 1997). Furthermore, many of these bodies have potassic affinities, which raises the possibility that migmatization and the K-rich metasomatism observed in many of the Kola xenoliths are related events; indeed, metasomatism may have facilitated migmatization in some cases.

Timing of metasomatism

Xenoliths containing veins (435-2, N57) or larger modal abundances of mica (e.g. 436-11) provide physical evidence for introduction of K-rich fluids into the lower crust. $^{87}Sr/^{86}Sr$ vs $^{87}Rb/^{86}Sr$ data for 436-11 suggest that the K-rich metasomatism may have occurred at ~1·9 Ga (Fig. 6). The trend of the Kola xenoliths in a $^{208}Pb/^{204}Pb$ vs $^{206}Pb/^{204}Pb$ plot, which projects back to the Stacey & Kramers (1975) growth curve at ~1·7 Ga (Fig.

9b), also implies concurrent changes in rock chemistry. Perhaps most convincing are the $^{40}Ar/^{39}Ar$ UV laser data from sample 436-11, which suggest that the old 2·10 ± 0·10 Ga ages preserved in the grain cores are phlogopite formation ages and hence determine the age of metasomatism. Collectively, the data suggest that the timing of metasomatism was ~2·0 Ga (Fig. 11), similar to the timing of migmatization identified above. Clearly, these events are not precisely constrained from the available data, but they are consistent with migmatization and metasomatism being closely related in space and time in the lower crust beneath Kola at ~2·0 Ga. One possibility is that the metasomatism is related to the 2·0 Ga plume event identified by Puchtel *et al.* (1998). Indeed, it may have been this second plume event that provided the heat source for both the metasomatism and migmatization recorded in the Kola xenoliths.

The timing of emplacement of the coarse-grained pyroxenite veins (e.g. 435-2P) may have been synchronous with formation of the granulite protoliths, given their similarity in Nd model ages (Table 3). However, sample 435-2P contains metasomatic phlogopite assimilated from the granulite wall rock of 435-2E, so unless there was more than one K-rich metasomatic event, the pyroxenite vein must be slightly younger than the metasomatism.

Hornblende metasomatism is uncommon among the granulites (only sample 435-1 has a high modal abundance of amphibole), but it has affected some pyroxenites significantly. In the fine-grained amphibole pyroxenites (436-15a and 436-15b), pargasite makes up 40–50% of the rock. The amphibole pyroxenites are also clearly different isotopically from the granulites and the coarse-grained pyroxenites, having low $^{87}Sr/^{86}Sr$, high $^{143}Nd/^{144}Nd$ and relatively unradiogenic Pb isotope ratios (Figs 5, 6 and 9). Hornblendite xenoliths, which consist of pargasite ± apatite, and layered rocks consisting of alternations of pargasite and clinopyroxene, are also present in the Elovy locality and elsewhere in the Kola alkaline province (A. Beard, personal communication, 1999), and may represent an end-member of the process of hornblende metasomatism. Beard *et al.* (1996) suggested that the hornblendite xenoliths, which yield a ^{40}Ar–^{39}Ar step-heating plateau mean (unweighted) age of 394 ± 2 Ma, are related to unexposed Devonian intrusions in the lower crust. The fact that the fine-grained amphibole pyroxenites are most similar in isotopic composition to the host lamprophyres is consistent with this interpretation. Thus, at least two episodes of metasomatism were likely to have occurred in the Kola lower crust: an older (Proterozoic) one that introduced phlogopite and a younger (Devonian) one related to the host magmatism that caused the precipitation of amphibole.

Effects of metasomatism on the lower crust

One of the more striking features of the Kola lower-crustal xenolith suite is the evidence for an ancient (i.e. ~2·1 Ga) K-rich metasomatic event. What are the consequences of this ancient and long-term enrichment? Is this style of metasomatism unique to the Kola granulites, or do other xenoliths share this feature?

Evidence for metasomatism is most readily apparent in xenoliths that have abundant disseminated mica (e.g. 436-11, 435-2E), micaceous veins (e.g. N57) and/or veins of amphibole (e.g. 435-1). These samples show variable, but typically strong, enrichments in the LILE Rb, Ba and K, and the LREE relative to HREE (see Fig. 3) when compared with other xenoliths in the suite (e.g. N42). Less obvious are small increases in Nb and Ti. Compared with other Palaeoproterozoic rocks (Fig. 4), the average Kola granulite composition is less depleted in Nb relative to La, and the metasomatized sample 435-1 is one of the few Kola xenoliths that lacks a negative Ti anomaly (Fig. 3a).

The extremely high $^{87}Sr/^{86}Sr$ ratio (0·9564) for the strongly metasomatized sample 436-11, combined with a $^{143}Nd/^{144}Nd$ value (0·5123) higher than most other Kola xenoliths, is clearly due to the radiogenic ingrowth of ^{87}Sr and ^{143}Nd as a response to the very high $^{87}Rb/^{86}Sr$ ratio (9·024) and the relatively high $^{147}Sm/^{144}Nd$ ratio (0·1988) of this rock. It is unclear whether the phlogopite metasomatism is responsible for the high Sm/Nd as well as the high Rb/Sr ratio of this sample, but higher than average Rb/Sr and $^{87}Sr/^{86}Sr$ are also observed in the phlogopite-metasomatized granulite 435-2E.

Similarly, Fig. 9 shows that the Kola granulite xenoliths differ from most other Archaean–Proterozoic granulite xenoliths in that the majority of samples plot near or to the right of the geochron in $^{207}Pb/^{204}Pb$ vs $^{206}Pb/^{204}Pb$ plots, more closely resembling xenoliths from beneath Phanerozoic terranes (Fig. 9c). However, unlike Phanerozoic xenolith suites, many of the Kola granulites also have unusually radiogenic $^{208}Pb/^{204}Pb$ values that are almost unique among lower-crustal xenoliths (Fig. 9d). Thus, on the basis of their Pb isotopic composition, essentially all Kola granulite xenoliths evolved with time-integrated Th/Pb and Th/U greater than that of average crust (as represented by the Stacey & Kramers growth curve), and many evolved with high time-integrated U/Pb values as well. Whether the time-integrated enrichment in Th/Pb and Th/U is the result of phlogopite metasomatism is difficult to establish, although the strongly metasomatized sample 436-11 has the most radiogenic Pb isotope composition of any Kola lower-crustal xenolith (see Fig. 9). If the elevated time-integrated Th/Pb and U/Pb ratios are the result of metasomatism, the absence of such compositions in other suites may simply reflect

the fact that appreciable amounts of metasomatic minerals have not been reported in lower-crustal xenoliths from other Archaean and Proterozoic regions.

Comparison with other metasomatized lower-crustal xenoliths

Although metasomatism occurs commonly in mantle-derived ultramafic xenolith suites (Harte, 1987; Kempton, 1987; Hawkesworth *et al.*, 1990), there is little evidence for its widespread occurrence in the lower crust. Two notable exceptions are the amphibole-bearing plag + cpx ± gar ± opx granulites from the Eifel, Germany (Stosch & Lugmair, 1984) and the amphibole-bearing cpx + gar + plag ± opx granulites from north Queensland (Stolz & Davies, 1989). In both cases the metasomatic phase is amphibole, which constrasts with the Kola granulite xenoliths, where phlogopite is the predominant hydrous phase. However, Stolz & Davies (1989) reported enrichments in TiO_2, Al_2O_3, Na_2O, K_2O, Rb, Sr, Ba, Zr, Nb and the LREE in the metasomatized granulites—features that are remarkably similar to those observed in the Kola suite. U, Th and Pb contents were not determined, so it is not known whether the metasomatism produced strong enrichments in these elements and whether, with time, these rocks would evolve to radiogenic Pb isotope compositions like those seen in the Kola suite.

Another interesting aspect of the north Queensland xenolith suite is that it also includes mantle peridotites that are metasomatized but felsic and two-pyroxene granulites that are free of metasomatism. The felsic and two-pyroxene granulites are interpreted as coming from shallower levels in the crust than the garnet-bearing granulites, which suggests that metasomatism has been restricted to the lowermost part of the crust, near the crust–mantle boundary.

In this context it is interesting to note that there are strong similarities between the metasomatized Kola granulite xenoliths and mica-bearing ultramafic peridotites and glimmerites from the Archaean Wyoming craton (Carlson & Irving, 1994). Some of these peridotites have extremely radiogenic Pb isotope ratios, which has been attributed to the introduction of mica and monazite during a metasomatic event at 1·8 Ga. This suggests that similar styles of metasomatism may have occurred at similar times in the lower crust and/or upper mantle in both the Baltic and Wyoming cratons.

The similarity between the style of metasomatism observed in the Kola granulites and that seen in the Wyoming mantle peridotites—combined with the observation that such metasomatism is rare in other lower-crustal xenoliths—suggests that it may largely be restricted to the lowermost part of thick continental roots. Thus, as volatile-rich melts ascend through the mantle, one likely place for them to stall and crystallize mica ± monazite ± rutile is near the boundary between the upper mantle and lower continental crust. Consistent with this hypothesis is the observation of Stolz & Davies (1989) that only the highest pressure granulites in the Queensland xenolith suite had undergone amphibole metasomatism. However, if this type of metasomatism is restricted to the lowermost part of thick continental crustal roots, as suggested by the Kola granulites and Wyoming glimmerites, it may be difficult to preserve, as it occurs in the part of the crust most likely to be delaminated and lost from areas that continue to be tectonically or magmatically active.

Significance of unsupported Pb isotope ratios

Figure 8 shows that the $^{206}Pb/^{204}Pb$ ratios in the xenoliths are unsupported by the present-day $^{238}U/^{204}Pb$, and Tables 4, 5 and 7 show that in most cases abundances of U, Th and K are at present low. This situation does not appear to be a direct effect of metasomatism, nor a consequence of contamination by the host lavas. If we accept that the array in the $^{207}Pb/^{204}Pb$ vs $^{206}Pb/^{204}Pb$ plot (Fig. 7a) has age signifiance, then the implied U and Th loss could not have taken place very long before exhumation. We cannot entirely rule out the possibility that the inverse relationship between U/Pb and isotopic composition is a mixing array between two source components, but one of the more intriguing aspects of the data in Fig. 8 is that the samples with the lowest measured U/Pb, but the most radiogenic Pb isotopic compositions (implying the highest time-integrated U/Pb and Th/Pb), are the 'eclogitic' granulites that have been interpreted as restites from a partial melting event (Kempton *et al.*, 1995).

In some aspects this association is similar to the LREE enrichment of some mantle peridotite xenoliths that have undergone cryptic metasomatism. That is, in most mantle xenolith suites, the greatest degree of LREE to HREE enrichment tends to occur in the most depleted rocks (Downes & Dupuy, 1987; Kempton, 1987); this relationship has been attributed to a chromatographic effect during migration of fluids and/or melts through the mantle (Navon & Stolper, 1987). However, metasomatism of the Kola granulites differs from cryptic metasomatism observed in some peridotites in that the primary minerals of the granulites (i.e. plagioclase, pyroxene and garnet) are not enriched in U and Th (Table 4). Instead, these samples must have originally contained greater modal abundances of U- and Th-rich metasomatic minerals (i.e. more directly analogous to modal metasomatism). If this is correct, the negative trend in Fig. 8 also implies that these metasomatic phases are more readily lost from the feldspar-poor lithologies—leaving them currently with the lower U/Pb.

This process may have been mineralogically controlled during metamorphism or migmatization. Ayers & Watson

(1991) argued that monazite and rutile would exert control as 'residual phases' during aqueous fluid metasomatism, potentially leaving the rock with high Th/Pb and Th/U. However, there is currently no obvious connection between radiogenic Pb isotope compositions and the modal abundance of rutile—and monazite has been identified only in sample N43. Furthermore, to generate the negative trend observed in Fig. 8 in this way, most of the rutile and/or monazite would have to become unstable just before exhumation by the host magma; yet there is no indication of metamorphism or migmatization at 380 Ma. However, Finger *et al.* (1998) have suggested that the stability of monazite depends strongly on lithological composition. Thus, if monazite was originally present in most samples, it could have been destabilized by the amphibole metasomatic event at ~380 Ma. The strongly discordant composition of rutile from sample 16/89 in a U/Pb concordia plot (Fig. 7f) does reflect severe disturbance of this mineral's isotopic system, which presumably occurred at the time of incorporation of the xenolith in the host lamprophyre. It should be noted that, in contrast, the coexisting garnet appears to have remained a closed system. Clearly, more work is required to understand how and when the Kola lower crust became open to Th and U loss.

Comparison of the Kola granulite xenoliths with lower-crustal xenoliths worldwide

The data presented in this paper suggest that the Kola granulite xenoliths represent the lower crust of a Palaeoproterozoic LIP, but are these rocks typical of Archaean and Palaeoproterozoic lower crust? Do the mafic granulite xenoliths of the northern Baltic Shield resemble xenoliths from other Archaean and Proterozoic regions? How does their origin and evolution compare with that of lower-crust formation proposed for Phanerozoic suites?

Mineralogically similar xenoliths have been reported from elsewhere in the cratonic parts of Europe, e.g. in Devonian lamprophyres in Belarus (Markwick *et al.*, 2001), in Palaeozoic kimberlites from the Arkhangelsk region (Markwick & Downes, 2000) and in late Proterozoic kimberlites of west Greenland (D. Garrit, personal communication, 1999). Particularly distinctive is the presence of large rutile grains and abundant garnet. The Kola xenoliths are also similar in mineralogical composition to the rutile-bearing garnet granulites from Lesotho (Rogers, 1977); however, in contrast to Kola, the Lesotho xenoliths have positive Eu anomalies and are considered to be magmatic cumulates (Rogers & Hawkesworth, 1982). Similar garnet granulites associated with eclogites have been reported from the West African shield (Toft *et al.*, 1989), the Kaapvaal craton (Huang *et al.*, 1995), Calcutteroo, southern Australia (McCulloch *et al.*, 1982), the Slave Province in northern Canada (Davis, 1997), the Superior Craton (Moser & Heaman, 1997), Montana (Collerson *et al.*, 1988; Joswiak, 1992) and Siberia (Shatsky *et al.*, 1990; Neymark *et al.*, 1992). Thus, high-pressure granulite xenoliths seem to be common in regions of ancient continental crust or Archaean cratons. Whether any were formed as part of a large igneous province is a question for future research.

The mafic protoliths of the Kola granulites probably formed in a manner analogous to Phanerozoic lower-crustal rocks, i.e. by basaltic underplating, but some of the distinctive features of the Kola granulite xenoliths may reflect its history as the lower crust of an ancient LIP. For example, Phanerozoic suites are typically lower-pressure, two-pyroxene and pyroxene + plagioclase granulites thought to be related to underplating of mantle-derived mafic magmas onto the base of extending (i.e. thin) continental crust by melts generated from upwelling of asthenospheric mantle (Rudnick *et al.*, 1986; Kempton *et al.*, 1990; Downes, 1993). In contrast, the predominance of garnet-rich mineral assemblages beneath Kola is consistent with a higher-pressure petrogenesis because of the thicker crust associated with LIPs. The higher temperatures associated with an ascending plume would also lead to more magnesian parental magmas, and the plume source would probably mean that these were LREE enriched.

Similarly, although partial melting of metasediments is recorded or inferred in Phanerozoic xenolith suites (e.g. Downes *et al.*, 1991), there is no evidence that conditions are suitable for migmatization of mafic igneous crust. In the case of Kola, there is evidence for just such a partial melting event in the form of migmatitic metaigneous granulites (e.g. N41-7, N57). Metasomatism may have induced, or at least facilitated, the migmatization. Metasomatism in Phanerozoic xenolith suites appears to be rare in general and dominated by introduction of modal amphibole where observed (Stosch & Lugmair, 1984; Stolz & Davies, 1989). In contrast, K-rich (i.e. mica-rich) metasomatism of the lowermost crust–mantle boundary may be common for thick continental roots, although these are probably lost through delamination and recycling in tectonically active areas, and may only rarely be preserved.

In summary, the Kola lower-crustal xenoliths may be the first such suite from a recognized Palaeoproterozoic LIP to have been studied in petrological detail. Evidence is mounting that other cratons have undergone similar Archaean and/or Proterozoic flood basalt magmatism. Given the temporal link between 2·4 Ga magmatism in the Superior, Wyoming and Karelian cratons proposed by Heaman (1997) and Vogel *et al.* (1998), similar processes of crystallization, metasomatism and migmatization may be recorded in the lower-crustal xenolith suites from these cratons. It may be through processes

similar to those recorded in the Kola xenoliths that predominantly mafic Archaean–Palaeoproterozoic LIPs are converted into continental crust. Whether or not the record of these processes is preserved is another question. It may be that these features are seldom observed because they become overprinted in tectonically active areas. Alternatively, the lowermost part of the crust may simply be delaminated during compressional tectonic events, and the record of these processes lost (Kay & Kay, 1991; Kempton & Harmon, 1992).

CONCLUSIONS

Garnet granulite xenoliths from the Kola Peninsula are interpreted as the high-grade metamorphic equivalents of continental flood tholeiite magmas. Similarities in major and trace element systematics suggest that they formed in response to the same major igneous event that affected the northern Baltic Shield in early Proterozoic times (~2·4–2·5 Ga). They thus represent the first well-studied lower crust of a Palaeoproterozoic LIP.

Processes that can be inferred to have occurred in the lower crust of the Kola Peninsula include: (1) underplating by mafic plume magmas; (2) K-rich (phlogopite) metasomatism; (3) formation of banded gneissic textures and migmatization; (4) alkaline (i.e. hornblende) metasomatism; and (5) loss of U–Th before exhumation in Devonian time. Formation of two different types of pyroxenites (fine-grained amphibole pyroxenites and coarse-grained pyroxenites) also occurred. The coarse-grained pyroxenites are probably Proterozoic in age, but younger than the granulite protoliths; they are certainly no older than the K-rich metasomatic event. The fine-grained amphibole pyroxenites relate to much younger magmatic activity, probably the Devonian alkaline event.

The unusual radiogenic Pb-isotope compositions of the xenoliths are probably the product of an ancient metasomatic event and not a function of initial protolith composition. Athough not well constrained, the metasomatic fluids may have originated from a second plume that arrived beneath Kola at ~2 Ga. Further detailed geochronology will be required to determine just how closely spaced in time are the metasomatism and migmatism. The data presented here indicate that the lower crust has not been uniformly depleted in U and Th relative to Pb since ancient times; instead, Th/Pb, Th/U and U/Pb ratios may locally have been elevated relative to that of average crust and mantle for at least 2 b.y.

The Kola suite provides evidence for partial melting of mafic crust (i.e. siliceous granulites) and restite formation (i.e. 'eclogitic' granulites), which occurred at ~2 Ga. These processes may be analogous to those required to convert Archaean LIP-generated proto-continents into continental crust.

ACKNOWLEDGEMENTS

We are grateful to Jean-Louis Bodinier, Greg Snyder and Larry Heaman for comments on an early draft version of this paper. Thorough reviews by John Tarney, Heinz Stosch and Cin Ty-Lee helped us to improve the clarity of our presentation. Thanks are due to Claire Grater (Royal Holloway, University of London) who provided some of the REE analyses, Dodie James (University of Edinburgh) for some of the XRF analyses, Paul Mason (NERC ICPMS facility) for help with the ICPMS analyses, Alexander Nemchin for help with Sm–Nd and Rb–Sr analyses at IPGG, Andy Beard for reconnaissance probe analyses, and Simon Kelly (Open University) for providing access to the UV laser $^{40}Ar/^{39}Ar$ facility and running the standards. Discussions with Dorte Garrit (Copenhagen), Svetlana Bogdanova (Lund), Valery Vetrin (Apatity), Andy Markwick (Birkbeck) and Steve Noble (NIGL) about the geochronology and nature of the lower crust of Archaean and Proterozoic terranes were very helpful. This work was supported by NERC, the Royal Society, Birkbeck College Research Fund and grant RFBR N 98-05-64458. This is NIGL Publication 371.

REFERENCES

Abbott, D. & Mooney, W. (1995). The structural and geochemical evolution of the continental crust—support for the oceanic plateau model of crustal growth. *Reviews of Geophysics* **33**, 231–242.

Alapieti, T. T., Filén, B. A., Lahtinen, J. J., Lavrov, M. M., Smolkin, V. F. & Voitsekhovsky, S. N. (1990). Early Proterozoic layered intrusions in the northeastern part of the Fennoscandian Shield. *Mineralogy and Petrology* **42**, 1–22.

Amelin, Y. V. & Neymark, L. A. (1998). Lead isotope geochemistry of Paleoproterozoic layered intrusions in the eastern Baltic Shield: inferences about magma sources and U–Th–Pb fractionation in the crust–mantle system. *Geochimica et Cosmochimica Acta* **62**, 493–505.

Amelin, Yu. V. & Semenov, V. S. (1996). Nd and Sr isotopic geochemistry of mafic layered intrusions in the eastern Baltic shield: implications for the evolution of Paleoproterozoic continental mafic magmas. *Contributions to Mineralogy and Petrology* **124**, 255–272.

Amelin, Yu. V., Heaman, L. M. & Semenov, V. S. (1995). U–Pb geochronology of layered mafic intrusions in the eastern Baltic Shield: implications for the timing and duration of Paleoproterozoic continental rifting. *Precambrian Research* **75**, 31–46.

Anderson, T. & Sundvoll, B. (1995). Neodymium isotope systematics of the mantle beneath the Baltic Shield: evidence for depleted mantle evolution since the Archean. *Lithos* **35**, 235–243.

Arnaud, N. O. & Kelley, S. P. (1997). Argon behaviour in gem-quality orthoclase from Madagascar: experiments and some consequences for $^{40}Ar/^{39}Ar$ geochronology. *Geochimica et Cosmochimica Acta* **61**, 3227–3255.

Ayers, J. C. & Watson, E. B. (1991). Solubility of apatite, monazite and rutile in supercritical aqueous fluids with implications for subduction zone chemistry. *Philosophical Transactions of the Royal Society, London, Series A* **335**, 365–375.

Azbel, I. Ya., Buyanov, A. F., Ionkis, V. T., Sharov, N. V. & Sharova, V. P. (1989). Crustal structure of the Kola Peninsula from deep seismic sounding data. *Tectonophysics* **162**, 87–99.

Beard, A. D., Downes, H., Vetrin, V., Kempton, P. D. & Maluski, H. (1996). Petrogenesis of Devonian lamprophyre and carbonatite minor intrusions, Kandalaksha Gulf (Kola Peninsula, Russia). *Lithos* **39**, 93–119.

Bernard-Griffiths, J., Peucat, J. J., Postaire, B., Vidal, Ph., Convert, J. Moreau, B. (1984). Isotopic data (U–Pb, Rb–Sr, Pb–Pb and Sm–Nd) on mafic granulites from Finnish Lapland. *Precambrian Research* **23**, 325–348.

Carlson, R. W. & Irving, A. J. (1994). Depletion and enrichment history of subcontinental lithospheric mantle: an Os, Sr, Nd and Pb isotopic study of ultramafic xenoliths from northwestern Wyoming Craton. *Earth and Planetary Science Letters* **126**, 457–472.

Chistyakov, A. V., Sukhanov, M. K., Bogatikov, O. A., Grinevich, N. G., Grokhovskaya, T. L., Lyapunov, S. M. & Sharkov, E. V. (1997). Features of distribution of the rare and rare-earth elements in the Burakovsky layered intrusion (southern Karelia). *Transactions (Doklady) of the Russian Academy of Sciences* **356**, 376–381.

Collerson, K. D., Hearn, B. C., MacDonald, R. A., Upton, B. F. & Park, J. G. (1988). Granulite xenoliths from the Bearpaw Mountains, Montana: constraints on the character and evolution of lower continental crust. *Terra Cognita* **8**, 270.

Davis, W. J. (1997). U–Pb zircon and rutile ages from granulite xenoliths in the Slave province: evidence for mafic magmatism in the lower crust coincident with Proterozoic dike swarms. *Geology* **25**, 343–346.

DePaolo, D. J., Linn, A. M. & Schubert, G. (1991). The continental crustal age distribution: methods of determining mantle separation ages from Sm–Nd isotopic data and application to the southwestern United States. *Journal of Geophysical Research* **96**, 2071–2088.

Downes, H. (1993). The nature of the lower continental crust of Europe: petrological and geochemical evidence from xenoliths. *Physics of the Earth and Planetary Interiors* **79**, 195–218.

Downes, H. & Dupuy, C. (1987). Textural, isotopic and REE variations in spinel peridotite xenoliths, Massif Central, France. *Earth and Planetary Science Letters* **82**, 121–135.

Downes, H., Kempton, P. D., Briot, D., Harmon, R. S. & Leyreloup, A. F. (1991). Lower crustal compositions and processes: Pb and O isotope evidence from granulite facies xenoliths, French Massif Central. *Earth and Planetary Science Letters* **102**, 342–357.

Finger, F., Broska, I., Roberts, M. & Schermaier, A. (1998). Replacement of primary monazite by apatite–allanite–epidote coronas in an amphibolite facies granite gneiss from the eastern Alps. *American Mineralogist* **83**, 248–258.

Glebovitsky, V. A. (1997). *The Early Precambrian of Russia*. Amsterdam: Harwood.

Harte, B. (1987). Metasomatic events recorded in mantle xenoliths: an overview. In: Nixon, P. H. (ed.) *Mantle Xenoliths*. Chichester: John Wiley.

Hawkesworth, C. J., Erlank, A. J., Kempton, P. D. & Waters, F. G. (1990). Mantle metasomatism: isotope and trace-element trends in xenoliths from Kimberley, South Africa. *Chemical Geology* **85**, 19–34.

Heaman, L. M. (1997). Global mafic magmatism at 2·45 Ga: remnants of an ancient large igneous province? *Geology* **25**, 299–302.

Higgins, S. J., Snyder, G. A., Mitchel, J. N., Taylor, L. A., Sharkov, E. V., Bogatikov, O. A., Grokhovskaya, T. L., Chistyakov, A. V., Ganin, V. A. & Grinevich, N. G. (1996). Petrology of the early Proterozoic Burakovsky layered intrusion, southern Karelia, Russia: mineral and whole-rock major-element chemistry. *Canadian Journal of Earth Sciences* **34**, 390–406.

Huang, Y.-M., Van Calsteren, P. & Hawkesworth, C. J. (1995). The evolution of the lithosphere in southern Africa: a perspective on the basic granulite xenoliths from kimberlites in South Africa. *Geochimica et Cosmochimica Acta* **59**, 4905–4920.

Joswiak, D. (1992). Composition and evolution of the lower crust, central Montana, evidence from granulite xenoliths. M.Sc. thesis, University of Washington, Seattle.

Kay, R. W. & Kay, S. M. (1991). Creation and destruction of lower continental crust. *Geologische Rundschau* **80**(2), 259–278.

Kelley, S. P., Arnaud, N. O. & Turner, S. P. (1994). High spatial $^{40}Ar/^{39}Ar$ investigations using an ultra-violet laser probe extraction technique. *Geochimica et Cosmochimica Acta* **58**, 3519–3525.

Kempton, P. D. (1987). Mineralogical and geochemical evidence for differing styles of metasomatism in spinel lherzolite xenoliths: enriched mantle source regions for basalts? In: Menzies, M. A. & Hawkesworth, C. J. (eds) *Mantle Metasomatism*. New York: Academic Press, pp. 45–89.

Kempton, P. D. (1995). Common Pb chemical procedures for silicate rocks and minerals, methods of data correction and an assessment of data quality at the NERC Isotope Geosciences Laboratory. NIGL Report Series, No. 78, 26 pp.

Kempton, P. D. & Harmon, R. S. (1992). Oxygen isotope evidence for large-scale hybridization of the lower crust during magmatic underplating. *Geochimica et Cosmochimica Acta* **56**, 971–986.

Kempton, P. D., Harmon, R. S., Hawkesworth, C. J. & Moorbath, S. (1990). Petrology and geochemistry of lower crustal granulites from the Geronimo Volcanic Field, southeastern Arizona. *Geochimica et Cosmochimica Acta* **54**, 3401–3426.

Kempton, P. D., Downes, H., Sharkov, E. V., Vetrin, V. R., Ionov, D. A., Carswell, D. A. & Beard, A. (1995). Petrology and geochemistry of xenoliths from the northern Baltic Shield: evidence for partial melting and metasomatism in the lower crust beneath an Archaean terrane. *Lithos* **36**, 157–184.

Kramm, U., Kogarko, L. N., Kononova, V. A. & Variainen, H. (1993). The Kola Alkaline Province of the CIS and Finland: precise Rb–Sr ages define 380–360 Ma age range for all magmatism. *Lithos* **30**, 33–44.

Leeman, W. P., Menzies, M. A., Mattey, D. J. & Embree, G. F. (1985). Strontium, neodymium and lead isotopic compositions of deep crustal xenoliths from the Snake River Plain: evidence for Archean basement. *Earth and Planetary Science Letters* **75**, 354–368.

Lobach-Zhuchenko, S. B., Arestova, N. A., Chekulaev, V. P., Levsky, L. K., Bogomolov, E. S. & Krylov, I. N. (1998). Geochemistry and petrology of 2·40–2·45 Ga magmatic rocks in the north-western Belomorian Belt, Fennoscandian Shield, Russia. *Precambrian Research* **92**, 223–250.

Ludwig, K. R. (1998). *Isoplot/Ex*. Berkeley Geochronology Center, Special Publication No. 1, 43 pp.

Manhes, G., Minster, I. F. & Allègre, C. J. (1978). Comparative uranium–thorium–lead and rubidium–strontium study of the Saint Severin amphoterite: consequences for early solar system chronology. *Earth and Planetary Science Letters* **39**, 14–24.

Markwick, A. J. W. & Downes, H. (2000). Lower crustal xenoliths from Arkhangelsk kimberlite pipes: petrological, geochemical and geophysical constraints. *Lithos* **51**, 135–151.

Markwick, A. J. W., Downes, H. & Veretennikov, N. (2001). The lower crust of S.E. Belarus: petrological, geophysical and geochemical constraints from xenoliths. *Tectonophysics* (in press).

McCulloch, M. T., Arculus, R. J., Chappell, B. W. & Ferguson, J. (1982). Isotopic and geochemical studies of nodules in kimberlites have implications for the lower continental crust. *Nature* **300**, 166–169.

McDougall, I. & Harrison, T. M. (1988). *Geochronology and Thermochronology by the $^{40}Ar/^{39}Ar$ Method*. Oxford: Oxford University Press.

Mitrofanov, F. P. (1995). *Geology of the Kola Peninsula (Baltic Shield)*. Apatity, Kola Science Publication, 144 pp.

Moser, D. E. & Heaman, L. M. (1997). Proterozoic zircon growth in Archean lower crustal xenoliths, southern Superior craton—a consequence of Matachewan ocean opening. *Contributions to Mineralogy and Petrology* **128**, 164–175.

Navon, O. & Stolper, E. (1987). Chemical consequences of melt percolation—the upper mantle as a chromatographic column. *Journal of Geology* **95**, 285–307.

Neymark, L. A., Nemchin, A. A., Rozen, O. M., Serenko, V. P., Spetsius, V. P. & Shuleshko, I. K. (1992). Sm–Nd isotope systematics in the lower crust xenoliths from kimberlites of Yakutia. *Doklady Rossiyskoy Akademii Nauk* **327**, 374–378.

Neymark, L. A., Kovach, V. P. & Nemchin, A. A. (1993*a*). Late Archean intrusive complexes in the Olekma granite–greenstone terrain (Eastern Siberia): geochemical and isotopic study. *Precambrian Research* **62**, 453–472.

Neymark, L. A., Nemchin, A. A., Vetrin, V. P. & Sal'nikova, Ye. B. (1993*b*). Sm–Nd and Pb–Pb isotope systems in lower-crustal xenoliths from dikes and explosion pipes in the southern part of the Kola Peninsula. *Doklady Rossiyskoy Akademii Nauk* **329**, 781–784.

Neymark, L. A., Amelin, Yu., V. & Larin, A. M. (1994). Pb–Nd–Sr isotopic and geochemical constraints on the origin of the 1·54–1·56 Ga Salmi rapakivi granite–anorthosite batholith (Karelia, Russia). *Mineralogy and Petrology* **50**, 173–193.

Patchett, J. & Kouvo, O. (1986). Origin of continental crust of 1·9–1·7 Ga age: Nd isotopes and U–Pb zircon ages in the Svecokarelian terrain of south Finland. *Contributions to Mineralogy and Petrology* **92**, 1–12.

Pearson, D. G., Kelley, S. P., Pokhilenko, N. P. & Boyd, F. R. (1997). Laser $^{40}Ar/^{39}Ar$ analyses of phlogopites from Southern Africa and Siberian kimberlites and their xenoliths: constraints on eruption ages, melt degassing and mantle volatile compositions. *Russian Journal of Geology and Geophysics* **38**, 106–117.

Phillips, D. (1990). Argon isotope and halogen chemistry of phlogopite from South African kimberlites: a combined step-heating, laser probe, electron microprobe and TEM study. *Chemical Geology (Isotope Geosciences Section)* **87**, 71–98.

Phillips, D. & Onstott, T. C. (1986). Application of $^{36}Ar/^{40}Ar$ versus $^{39}Ar/^{40}Ar$ correlation diagrams to the $^{40}Ar/^{39}Ar$ spectra of phlogopites from Southern African kimberlites. *Geophysical Research Letters* **13**, 689–692.

Phillips, D. & Onstott, T. C. (1988). Argon isotopic zoning in mantle phlogopite. *Geology* **16**, 542–546.

Puchtel, I. S., Hofmann, A. W., Mezger, K., Shchipansky, A. A., Kulikov, V. S. & Kulikova, V. V. (1996). Petrology of a 2·41 Ga remarkably fresh komatiitic basalt lava lake in Lion Hills, central Vetreny Belt, Baltic Shield. *Contributions to Mineralogy and Petrology* **124**, 273–290.

Puchtel, I. S., Haase, K. M., Hofmann, A. W., Chauvel, C., Kulikov, V. S., Garbe-Schönberg, C.-D. & Nemchin, A. A. (1997). Petrology and geochemistry of crustally contaminated komatiitic basalts from the Vetreny Belt, southeastern Baltic Shield: evidence for an early Proterozoic mantle plume beneath rifted Archean continental lithosphere. *Geochimica et Cosmochimica Acta* **61**, 1205–1222.

Puchtel, I. S., Arndt, N. T., Hofmann, A. W., Haase, K. M., Kröner, A., Kulikov, V. S., Kulikova, V. V., Garbe-Schönberg, C.-D. & Nemchin, A. A. (1998). Petrology of mafic lavas within the Onega plateau, central Karelia: evidence for 2·0 Ga plume-related continental crustal growth in the Baltic Shield. *Contributions to Mineralogy and Petrology* **130**, 134–153.

Rogers, N. W. (1977). Granulite xenoliths from Lesotho kimberlites and the lower continental crust. *Nature* **270**, 681–684.

Rogers, N. W. & Hawkesworth, C. J. (1982). Proterozoic age and cumulate origin for granulite xenoliths, Lesotho. *Nature* **299**, 409–413.

Royse, K. R., Kempton, P. D. & Darbyshire, F. D. (1998). Procedure for the analysis of rubidium–strontium and samarium–neodymium isotopes at the NERC Isotope Geosciences Laboratory. NIGL Report Series, No. 121, 28 pp.

Rudnick, R. L. (1992). Xenoliths—samples of the lower continental crust. In: Fountain, D. M., Arculus, R. & Kay, R. W. (eds) *Continental Lower Crust*. New York: Elsevier, pp. 269–316.

Rudnick, R. L. & Fountain, D. M. (1995). Nature and composition of the continental crust: a lower crustal perspective. *Reviews of Geophysics* **33**, 267–309.

Rudnick, R. L., McDonough, W. F., McCulloch, M. T. & Taylor, S. R. (1986). Lower crustal xenoliths from Queensland, Australia: evidence for deep crustal assimilation and fractionation of continental basalts. *Geochimica et Cosmochimica Acta* **50**, 1099–1115.

Sharkov, E. V., Lyakhovich, Vl. V. & Ledneva, G. V. (1994). Petrology of the early Proterozoic drusite complex, White Sea Region, with reference to the Pezhostrov Massif, North Karelia. *Petrology* **2**, 454–474.

Sharkov, E. V., Bogatikov, O. A., Grokhovskaya, T. L., Chisyakov, A. V., Ganin, V. A., Grinevich, N. G., Snyder, G. A. & Taylor, L. A. (1995). Petrology and Ni–Cu–Cr–PGE mineralization of the largest mafic pluton in Europe: the early Proterozoic Burakovsky layered intrusion, Karelia, Russia. In: Snyder, G. A., Neal, C. R. & Ernst, W. G. (eds) *Planetary Petrology and Geochemistry: The Lawrence A. Taylor 60th Birthday Volume. Geological Society of America, International Book Series, Vol. 2*. Columbia, MD: Bellwether, pp. 53–73.

Sharkov, E. V., Smolkin, V. F. & Krassivskaya, I. S. (1997). Early Proterozoic igneous province of siliceous high-Mg boninite-like rocks in the eastern Baltic Shield. *Petrology* **5**, 448–465.

Sharkov, E. V., Snyder, G. A., Taylor, L. A. & Zinger, T. F. (1999). An early Proterozoic large igneous province in the eastern Baltic Shield: evidence from the mafic drusite complex, Belomorian Mobile Belt, Russia. *International Geology Review* **41**, 73–93.

Shatsky, V., Rudnick, R. L. & Jagoutz, E. (1990). Mafic granulites from Udachnaya pipe, Yakutia: samples of Archean lower crust? In: Sobolev, N. V. (ed.) *Deep Seated Magmatism and Evolution of Lithosphere of Siberian Platform*. Mirny: Siberian Branch, USSR Academy of Sciences.

Snyder, G. A., Taylor, L. A., Jerde, E. A., Sharkov, E. V., Liachovitch, V. V. & Ledneva, G. V. (1995). Petrology and chemistry of an early Proterozoic lherzolite–gabbronorite–anorthosite pluton of the White Sea Complex, northern Karelia, Russia. *International Geology Review* **37**, 547–560.

Snyder, G. A., Higgins, S. J., Taylor, L. A., Jain, J., Neal, C. R. & Sharkov, E. (1996). Archean enriched mantle beneath the Baltic shield: rare-earth-element evidence from the Burakovsky layered intrusion, southern Karelia, Russia. *International Geology Review* **38**, 389–404.

Stacey, J. S. & Kramers, J. D. (1975). Approximation of terrestrial lead isotope evolution by a two-stage model. *Earth and Planetary Science Letters* **26**, 207–221.

Stein, M. & Goldstein, S. L. (1996). From plume head to continental lithosphere in the Arabian–Nubian Shield. *Nature* **382**, 773–778.

Stein, M. & Hofmann, A. W. (1994). Mantle plumes and episodic crustal growth. *Nature* **372**, 63–68.

Stolz, A. J. & Davies, G. R. (1989). Metasomatised lower crustal and upper mantle xenoliths from north Queensland: chemical and isotopic evidence bearing on the composition and source of the fluid phase. *Geochimica et Cosmochimica Acta* **53**, 649–660.

Stosch, H.-G. & Lugmair, G. W. (1984). Evolution of the lower continental crust: granulite facies xenoliths from the Eifel, West Germany. *Nature* **311**, 368–370.

Sun, S. S. & McDonough, W. F. (1989). Chemical and isotopic systematics of oceanic basalts: implications for mantle composition and processes. In: Saunders, A. D. & Norry, M. J. (eds) *Magmatism in the Ocean Basins. Geological Society, London, Special Publications* **42**, 313–345.

Taylor, S. R. (1967). The origin and growth of continents. *Tectonophysics* **4**, 17–34.

Taylor, S. R. (1977). Island arc models and the composition of the continental crust. *Maurice Ewing Series, American Geophysical Union* **1**, 325–355.

Todt, W., Cliff, R. A., Hanser, A. & Hofmann, A. W. (1984). ^{202}Pb + ^{205}Pb double spike for lead isotopic analyses. *Terra Cognita* **4**, 209.

Toft, P. B., Hills, D. V. & Haggerty, S. E. (1989). Crustal evolution and the granulite to eclogite transition in xenoliths from kimberlites in the West African Craton. *Tectonophysics* **161**, 213–231.

Vetrin, V. R. & Nemchin, A. A. (1998). The U–Pb age of zircon from a granulite xenolith of granulite in the diatreme on Elovy island (the southern Kola Peninsula). *Doklady Earth Sciences* **359**(A), 454–456.

Vogel, D. C., Vuollo, J. I., Alapieti, T. T. & James, R. S. (1998). Tectonic, stratigraphic and geochemical comparisons between ca. 2500–2440 Ma mafic igneous events in the Canadian and Fennoscandian Shields. *Precambrian Research* **92**, 89–116.

Wartho, J.-A., Kelley, S. P., Brooker, R. A., Carroll, M. R., Villa, I. M. & Lee, M. R. (1999). Direct measurement of Ar diffusion profiles in a gem-quality Madagascar K-feldspar using the Ultra-Violet Laser Ablation Micro-Probe (UVLAMP). *Earth and Planetary Science Letters* **170**, 141–153.

White, R. S., Spence, G. D., Fowler, S. R., McKenzie, D. P., Westbrook, G. K. & Bowen, A. N. (1987). Magmatism at rifted continental margins. *Nature* **330**, 439–444.

White, R. V., Tarney, J., Kerr, A. C., Saunders, A. D., Kempton, P. D., Pringle, M. S. & Klaver, G. T. (1999). Modification of an oceanic plateau, Aruba, Dutch Caribbean: implications for the generation of continental crust. *Lithos* **46**, 43–68.